HELSINKI UNIVERSITY OF TECHNOLOGY
Faculty of Electronic, Communications and Automation

Juhani Kataja

ON NUMERICS OF BOUNDARY INTEGRAL EQUATIONS IN ELECTROMAGNETIC SCATTERING

Thesis submitted for examination for the degree of Master of Science in Technology

Espoo 14.2.2008

Thesis supervisor:

Prof. Keijo Nikoskinen

Thesis instructor:

Prof. Jukka Sarvas

TEKNILLINEN KORKEAKOULU

DIPLOMITYÖN TIIVISTELMÄ

Tekijä: Juhani Kataja

Työn nimi: Sähkömagnettisen sironnan reunaintegraaliyhtälöiden numeriikasta

Päivämäärä: 14.2.2008 Kieli: Englanti Sivumäärä: 6+52

Tiedekunta: Elektroniikan, tietoliikenteen ja automaation tiedekunta

Professuuri: Sähkömagnetiikka Koodi: S-96

Valvoja: Prof. Keijo Nikoskinen

Ohjaaja: Prof. Jukka Sarvas

Tässä työssä johdetaan Stratton-Chu kaavoista ja niihin liittyvien potentiaalien raja-arvokaavoista lähtien EFIE, MFIE, CFIE ja Müllerin formulaatiot sähkömagneettisen sironnan integraaliyhtälöille. Näiden avulla rakennetaan C- ja MATLAB -ympäristössä RWG-elementtejä käyttäen numeeriset ratkaisuohjelmat EFIE, MFIE sekä CFIE -formulaatioille täysjohtavan kappaleen tapauksessa sekä Müllerin formulaatiolle dielektrisen kappaleen tapauksessa. Tämän toteutuksen avulla tutkitaan eri formulaatioiden käyttäytymistä numeerisesti.

Erityisesti näytettiin numeerisesti pintaintegraaliyhtälöiden sisäresonanssi- ja matalan taajuuden ongelmien esiintyminen. Lisäksi näytettiin numeerisesti, että nämä ongelmat poistuvat sopivalla formulaatiolla.

Lopuksi sirontayhtälön ratkaisijaa käytettiin pitkän kapean levyantennin muodon optimointiin antennin hyvän suuntaavuuden saavuttamiseksi. Tuloksena löydettiin muoto, joka on lähellä aikaisemmin tunnettua Landstorferin lanka-antennia sekä kaksi muuta muotoa, jotka poikkeavat huomattavasti Landstorferin antenneista.

Avainsanat: EFIE, MFIE, CFIE, Müller formulation,antenna shape optimisation

Author: Juhani Kataja

Title: On numerics of boundary integral equations in electromagnetic scattering

Date: 14.2.2008 Language: English Number of pages: 6+52

Faculty: Faculty of Electronic, Communications and Automation

Professorship: Electromagnetics Code: S-96

Supervisor: Prof. Keijo Nikoskinen

Instructor: Prof. Jukka Sarvas

The EFIE, MFIE, CFIE and Müller formulations for the surface integral equations were derived from the Stratton-Chu formulas and limit theorem of the double layer potential. Their numerical implementations were constructed using the RWG-elements in the C-language and MATLAB environments. EFIE, MFIE and CFIE were applied to a perfectly conducting scatterer, and the Müller formulation to a dielectric one.

The interior resonance problem and low frequency breakdown were rediscovered and the remedies discovered earlier were also presented.

The solver of the scattering problem was used to optimise the directivity of a long patch antenna. A shape was found that is similar to one found by Landstorfer for a wire antenna and two other shapes that differ noticeably from Landstrofer's antennas.

Keywords: EFIE, MFIE, CFIE, Müller formulation,antenna shape optimisation

Preface

I would like to thank professor Jukka Sarvas for patient instructing and encouragement. My thanks are also due to professor Keijo Nikoskinen for suggesting the topic on the Landstorfer antenna. I would also like to thank Seppo Järvenpää for pointing out the use of polynomials to represent RWG functions. Finally, I wish to express my gratitude towards Department of Radio Science and Engineering for providing me with a desk and a room where to work.

Espoo, 4.2.2008 Juhani Kataja

Contents

Symbols and abbreviations

List of symbols

$\mathbf{E}$	Electric field strength
$\mathbf{H}$	Magnetic field strength
$\mathbf{J}$	Electric current density or equivalent electric current density
$\mathbf{M}$	Magnetic current density or equivalent magnetic current density
$\mathbb{R}$	The real numbers
$\mathbb{C}$	The complex numbers
$\mathbb{R}^n$	Real normed space of dimension n
$\mathbb{C}^n$	Complex normed space of dimension n
$\|\|x\|\|$	Norm of x
$Im(z)$	The imaginary part of the complex number z
$Re(z)$	The real part of the complex number z
$\overline{z}$	The complex conjugate of the complex number z
$\mathcal{P}_n(X)$	The set of polynomials of order n on $X \subset \mathbb{R}^n$
$f \circ g$	Composition of functions f and g
δ_{ij}	The Kronecker delta, $\delta_{ij} = 1$ if $i = j$ and 0 otherwise
$\delta_{\mathbf{p}}$	The Dirac's delta distribution at $\mathbf{p}$

Introduction

The electromagnetic scattering problem of homogeneous bodies in a homogeneous space is one of the central problems in electromagnetics. It has applications for example in antenna simulation, wave guide simulation and radar problems. The scattering problem is formulated as an integral equation using Stratton-Chu formulas. However there is no single best way to write the integral equation formulation. Here the most common formulations are derived.

There are some nontrivial problems with the discretization of the integral equations. The arising linear system will have a fully populated coefficient matrix, thus the matrix memory requirement is $O(N^2)$, where N is the number of degrees of freedom. The matrix assembly is also computationally extremely intensive procedure, for the calculation of the matrix elements involves singular integrals, which must be treated properly.

The problem of calculation of singular integrals is described in articles [1], [2], [3] and [4]. However the implementation here is done calculating singular integrals involving Lagrange's linear basis functions as presented in [4]. The key idea is the same in both articles, however.

Having the machinery to implement the discrete version of the integral equation, different integral equation formulations are studied numerically. These formulations are EFIE, MFIE and CFIE for perfect electric conductor and the Müller formulation for dielectric object. It is found that, although, the matrix assembly of CFIE formulation is somewhat slower, the resulting matrix will have nice properties. Furthermore, the Müller formulation turns out to behave very well in GMRES [5], [6] iteration.

The EFIE solver can be used to calculate the directivity of an antenna, and thus using numerical optimisation schemes, it is possible to optimise the directivity of an antenna. For that end, the implementation must be made in some compiled language in order to achieve a reasonable iteration speed. The field must be calculated $O(N)$ times for every iteration step of the optimisation routine. Here N corresponds to the dimension of the space that represents the shape of the antenna.

Here the convergence of the discretized equation to the original one is not discussed and also we have excluded the discussion about the solution space where the original solution lies. Neither we have paid attention to the fact that, in the literature [7], the limit theorems are proved only for smooth surfaces.

Chapter 1

Preliminaries

The purpose of this chapter to give exposition to the mathematical notions that are used in solving electromagnetic scattering problems in this thesis.

The most important statements of this chapter are the Stratton-Chu formulas and the limit theorems. They are the key ingredients in deriving the different integral equation formulations for electromagnetic scattering problems.

1.1 Notation

The electromagnetic fields are denoted in the following way:

Symbol	Field
$\mathbf{E}$	Electric field
$\mathbf{H}$	Magnetic field
$\mathbf{J}$	Electric current or equivalent surface current
$\mathbf{M}$	Magnetic current or equivalent surface current

The real and complex numbers are denoted by $\mathbb{R}$ and $\mathbb{C}$, respectively. The imaginary unit is denoted by i and real and imaginary part of a complex number z is denoted by $Re(z)$ and $Im(z)$, respectively. The complex conjugate of a complex number z is denoted by $\overline{z}$.

The set of polynomials of order n on $X \subset \mathbb{R}^N$ is denoted by $\mathcal{P}_n(X)$.

Dot product $\mathbb{C}^n \times \mathbb{C}^n \to \mathbb{C}$ is defined by $a \cdot b := \sum_{k=1}^n a_k b_k$ and cross product $\mathbb{C}^3 \times \mathbb{C}^3 \to \mathbb{C}^3$ by $a \times b := [a_2 b_3 - a_3 b_2, b_3 a_1 - a_1 b_3, a_1 b_2 - b_2 a_1]$.

Integral of the function f over the set D is denoted by $\int_D f(\mathbf{r}) d\mathbf{r}$ and whether the integral is volume, surface or line integral depends on the context.

The sesquilinear form $\langle \cdot, \cdot \rangle$ on the fields $\mathbf{F}, \mathbf{G}$ on a surface S is defined by

$$\langle \mathbf{F}, \mathbf{G} \rangle = \int_S \overline{\mathbf{F}(\mathbf{r})} \cdot \mathbf{G}(\mathbf{r}) d\mathbf{r}.$$

The *interior* of the set S in a topological space X is denoted by $intS$ and *closure* is denoted by clS or $\overline{S}$. The *exterior* is denoted by $extS$ and it is the interior of the complement of clS in X.

The *support* of the function $f : X \to \mathbb{C}^n$ is defined by

$$supp(f) := cl\left\{x \in X \middle| f(x) \neq 0\right\}.$$

Latin lowcase letters i, j, k, l, m, n, p, q in sub- and superscripts generally denote integer indices except for Green's function g_k where it denotes the wavenumber.

The action of integers due to summation on finite linearly ordered index sets is defined in a natural rotational way so that the result is always in the index set. For example: if $n \in (1, 2, 3)$ then $n = 1 \Rightarrow n + 2 = 3,\ n = 2 \Rightarrow n + 2 = 1,\ n = 3 \Rightarrow n + 2 = 2$.

1.2 Maxwell's equations

In an inhomogeneous, isotropic, linear, temporally constant space the time harmonic Maxwell's equations, for time factor $e^{-i\omega t}$, $\omega > 0$, take the form [8], [9]

$$\begin{aligned} \nabla \times \mathbf{E} &= i\omega\mu\mathbf{H} - \mathbf{M}, && (1.1)\\ \nabla \times \mathbf{H} &= -i\omega\varepsilon\mathbf{E} + \mathbf{J}, && (1.2)\\ \nabla \cdot \mathbf{J} &= i\omega\rho, && (1.3)\\ \nabla \cdot (\mu\mathbf{H}) &= 0. && (1.4) \end{aligned}$$

Here $\varepsilon : \mathbb{R}^3 \to \mathbb{C}$ corresponds to the electric permittivity with $Im(\varepsilon) \geq 0$ and $Re(\varepsilon) > 0$, and $\mu : \mathbb{R}^3 \to \mathbb{R}^+$ corresponds to the magnetic permeability and ρ denotes the electric charge density distribution. If ε and μ are constant, then the equations (1.1-1.4) are said to be homogeneous.

Also the following equation holds

$$\nabla \cdot (\varepsilon\mathbf{E}) = \rho, \qquad (1.5)$$

for it is a consequence of equations (1.2) and (1.3).

One says that $\mathbf{E}$ and $\mathbf{H}$ solve the sourceless Maxwell's equations if they satisfy (1.1-1.4) for $\mathbf{J} = 0$ and $\mathbf{M} = 0$. From now on the equations (1.1-1.3) are considered as *the* Maxwell's equations unless stated otherwise.

1.3 Vector potentials and Stratton-Chu formulas

Let $\mathbf{A} : \mathbb{R}^3 \to \mathbb{C}^3$ and $\mathbf{F} : \mathbb{R}^3 \to \mathbb{C}^3$ be defined by

$$\mathbf{A}(\mathbf{r}) = \int_{\mathbb{R}^3} g_k(\mathbf{r}, \mathbf{r}')\mathbf{J}(\mathbf{r}')dV' \qquad (1.6)$$

and

$$\mathbf{F}(\mathbf{r}) = \int_{\mathbb{R}^3} g_k(\mathbf{r}, \mathbf{r}')\mathbf{M}(\mathbf{r}')dV', \tag{1.7}$$

respectively where $g_k : \mathbb{R}^3 \times \mathbb{R}^3 \to \mathbb{C}$ is defined by

$$g_k(\mathbf{r}, \mathbf{r}') = \frac{e^{ik||\mathbf{r}-\mathbf{r}'||}}{4\pi\,||\mathbf{r}-\mathbf{r}'||}, \tag{1.8}$$

ie. it is the fundamental solution, or Green's function, of the scalar Helmholtz equation with wavenumber k:

$$(\Delta + k^2) \int_{supp(f)} g_k(\mathbf{r}, \mathbf{r}')f(\mathbf{r}')d\mathbf{r}' = -f(\mathbf{r}).$$

Thus the components of $\mathbf{A}$ and $\mathbf{F}$ are solutions to scalar Helmholtz equation with right hand side being the components of $\mathbf{J}$ and $\mathbf{M}$:

$$(\Delta + k^2)\mathbf{A} = -\mathbf{J} \quad \text{and} \quad (\Delta + k^2)\mathbf{F} = -\mathbf{M}.$$

The subscript of g_k is left out when there is no possibility of confusion.

The functions $\mathbf{A}$ and $\mathbf{F}$ are called the electric and magnetic Hertz potentials, respectively.

The fields $\mathbf{E}$ and $\mathbf{H}$ given by

$$\mathbf{E}(\mathbf{r}) = -\frac{1}{i\omega\varepsilon}(\nabla\nabla\cdot + k^2)\mathbf{A}(\mathbf{r}) - \nabla \times \mathbf{F}(\mathbf{r}) \tag{1.9}$$

and

$$\mathbf{H}(\mathbf{r}) = -\frac{1}{i\omega\mu}(\nabla\nabla\cdot + k^2)\mathbf{F}(\mathbf{r}) + \nabla \times \mathbf{A}(\mathbf{r}) \tag{1.10}$$

satisfy the Maxwell's equations (1.1-1.3) with given current distributions $\mathbf{M}$ and $\mathbf{J}$ at frequency ω. The wave number k is defined by $k = \omega\sqrt{\varepsilon\mu}$ such a way that fields vanish at infinity, ie. $Im(k) \geq 0$. The proof consist of a straightforward calculation and the fact that that $\mathbf{A}$ and $\mathbf{F}$ satisfy vectorial Helmholtz's equation.

The fields obtained this way from the Hertz potentials also satisfy the Silver-Müller condition [7] and are thus admissible solutions to Maxwell's equations.

1.4 Surface integral representations

The key ingredients in deriving the surface integral equations are the Stratton-Chu formulas and certain limits of Hertz potentials to the surfaces which are the supports of the current distributions $\mathbf{J}$ and $\mathbf{M}$.

The presentation here follows that of in [8]. For more rigorous treatment, see [7] although notation differs in [7].

Let D be a bounded open set in $\mathbb{R}^3$ with a well-behaved boundary $S := \partial D$ and let $\mathbf{F}$ be a vector field $S \to \mathbb{C}^3$.

The integral operators S_k, K_k and D_k associated with S are defined by

$$(S_k\mathbf{F})(\mathbf{r}) = \int_S g_k(\mathbf{r},\mathbf{r}')\mathbf{F}(\mathbf{r}')d\mathbf{r}', \tag{1.11}$$

$$(K_k\mathbf{F})(\mathbf{r}) = \nabla \times \int_S g_k(\mathbf{r},\mathbf{r}')\mathbf{F}(\mathbf{r}')d\mathbf{r}' \tag{1.12}$$

and

$$(D_k\mathbf{F})(\mathbf{r}) = \nabla \times \nabla \times \int_S g_k(\mathbf{r},\mathbf{r}')\mathbf{F}(\mathbf{r}')d\mathbf{r}' \tag{1.13}$$

for $\mathbf{r} \notin S$.

Let $\hat{\mathbf{n}}$ be the unit outer normal to D and let $\mathbf{J}$ and $\mathbf{M}$ be defined by

$$\mathbf{J} := \hat{\mathbf{n}} \times \mathbf{H} \quad \text{and} \quad \mathbf{M} := -\hat{\mathbf{n}} \times \mathbf{E} \tag{1.14}$$

on S. For the rest of the thesis $\mathbf{J}$ and $\mathbf{M}$ denote the equivalent surface currents. If there are any subscripts on them they refer to the fields they are equivalent with, eg. $\mathbf{J}_s = \hat{\mathbf{n}} \times \mathbf{H}_s$.

The following identities also hold for $\mathbf{r} \notin S$:

$$\nabla \times \int_S g_k(\mathbf{r},\mathbf{r}')\mathbf{F}(\mathbf{r}')d\mathbf{r}' = \int_S \nabla g_k(\mathbf{r},\mathbf{r}') \times \mathbf{F}d\mathbf{r}'$$

and

$$\nabla \times \nabla \times \int_S g_k(\mathbf{r},\mathbf{r}')\mathbf{F}(\mathbf{r}')d\mathbf{r}' = \int_S (\nabla\nabla\cdot + k^2)g_k(\mathbf{r},\mathbf{r}')\mathbf{F}(\mathbf{r}')d\mathbf{r}.$$

These identities will be used without notice later.

With this notation the Stratton-Chu formulas [10] are stated as follows:

Theorem 1.1 *(Interior Stratton-Chu formulas) If* $\mathbf{E}$ *and* $\mathbf{H}$ *solve the sourceless homogeneous Maxwell's equations in* D*, then it holds*

$$\frac{-1}{i\omega\epsilon}(D_k\mathbf{J})(\mathbf{r}) - (K_k\mathbf{M})(\mathbf{r}) = \begin{cases} -\mathbf{E}(\mathbf{r}) & \text{if } \mathbf{r} \in D \\ 0 & \text{if } \mathbf{r} \in extD \end{cases} \tag{1.15}$$

and

$$\frac{-1}{i\omega\mu}(D_k\mathbf{M})(\mathbf{r}) + (K_k\mathbf{J})(\mathbf{r}) = \begin{cases} -\mathbf{H}(\mathbf{r}) & \text{if } \mathbf{r} \in D \\ 0 & \text{if } \mathbf{r} \in extD. \end{cases} \tag{1.16}$$

Theorem 1.2 *(Exterior Stratton-Chu formulas) If* $\mathbf{E}$ *and* $\mathbf{H}$ *solve the sourceless homogeneous Maxwell's equations in* $extD$ *and satisfy one of the Silver-Müller radiation conditions*

$$\mathbf{H} \times \mathbf{u}_\mathbf{r} - \mathbf{E} = o\left(\frac{1}{|\mathbf{r}|}\right), \quad \mathbf{r} \to \infty$$

or

$$\mathbf{E} \times \mathbf{u_r} + \mathbf{H} = o\left(\frac{1}{|\mathbf{r}|}\right), \quad \mathbf{r} \to \infty,$$

then it holds

$$\frac{-1}{i\omega\epsilon}(D_k\mathbf{J})(\mathbf{r}) - (K_k\mathbf{M})(\mathbf{r}) = \begin{cases} 0 & \text{if } \mathbf{r} \in D \\ \mathbf{E}(\mathbf{r}) & \text{if } \mathbf{r} \in extD \end{cases} \tag{1.17}$$

and

$$\frac{-1}{i\omega\mu}(D_k\mathbf{M})(\mathbf{r}) + (K_k\mathbf{J})(\mathbf{r}) = \begin{cases} 0 & \text{if } \mathbf{r} \in D \\ \mathbf{H}(\mathbf{r}) & \text{if } \mathbf{r} \in extD. \end{cases} \tag{1.18}$$

These theorems can be seen as a modern restatement of the Huygens's principle: The fields outside (or inside) of D due to sources inside (or outside) of D can be calculated from equivalent sources on S.

The integral operators $\tilde{K}_k$ and $\tilde{D}_k$ are defined on sufficiently smooth tangential vector fields $\mathbf{F}$ on S as follows:

$$\begin{aligned} (\tilde{K}_k\mathbf{F})(\mathbf{r}) &= \int_S \hat{\mathbf{n}} \times \nabla \times [g(\mathbf{r},\mathbf{r}')\mathbf{F}(\mathbf{r}')]d\mathbf{r}' \\ &= \int_S \hat{\mathbf{n}} \times [\nabla g(\mathbf{r},\mathbf{r}') \times \mathbf{F}(\mathbf{r}')]d\mathbf{r}' \end{aligned} \tag{1.19}$$

and

$$(\tilde{D}_k\mathbf{F})(\mathbf{r}) = p.v. \int_S \hat{\mathbf{n}} \times (\nabla\times)^2[g(\mathbf{r},\mathbf{r}')\mathbf{F}(\mathbf{r}')]d\mathbf{r}' \tag{1.20}$$

for $\mathbf{r} \in S$.

Using this notation the main limit theorem, used in the derivation of the basic integral equations, can be stated in the following way:

Theorem 1.3 *For a smooth tangential vector field* $\mathbf{F}$ *on a smooth surface* S *it holds:*

$$\lim_{h\to 0^{\pm}} (S_k\mathbf{F})(\mathbf{r} + h\hat{\mathbf{n}}(\mathbf{r})) = (S_k\mathbf{F})(\mathbf{r}), \tag{1.21}$$

$$\lim_{h\to 0^{\pm}} \hat{\mathbf{n}}(\mathbf{r}) \times (K_k\mathbf{F})(\mathbf{r} + h\hat{\mathbf{n}}(\mathbf{r})) = (\tilde{K}_k\mathbf{F})(\mathbf{r}) \pm \frac{1}{2}\mathbf{F}(\mathbf{r}) \tag{1.22}$$

and

$$\lim_{h\to 0^{\pm}} \hat{\mathbf{n}}(\mathbf{r}) \times (D_k\mathbf{F})(\mathbf{r} + h\hat{\mathbf{n}}(\mathbf{r})) = (\tilde{D}_k\mathbf{F})(\mathbf{r}). \tag{1.23}$$

For proofs and more detailed treatment on the theorems above see [7], [8].

The final formulations of the correct integral equations for different kinds of scatterers is only a matter of combining the above statements. The formulations and their derivations will be presented in Chapter 2 and Appendix A.

1.5 Finite elements

Finite elements are used to build finite dimensional function spaces on triangulated surfaces in $\mathbb{R}^3$. The discrete solutions to boundary integral equations are sought from these finite element spaces.

The superscripts in symbols generally refer to local indices and subscripts refer to global indices.

For the use of this thesis the following definition of finite element is used [11], [12]:

Definition 1.1 *A finite element is a triple* (T, Π, Σ)*, where* $T \subset \mathbb{R}^d$ *is a polyhedron,* Π *is a finite subspace of* $C(T)$ *and* Σ *is such a finite set of functionals on* Π*, that if for* $x, y \in \Pi$ *it holds* $f(x-y) = 0$ *for all* $f \in \Sigma$*, then* $x = y$*.*

Definition 1.2 *The* reference triangle $\hat{T}$ *is defined by*

$$\hat{T} = \left\{ \xi, \eta \in \mathbb{R}^2 \middle| \xi + \eta < 1,\ \xi, \eta > 0 \right\}.$$

Remark 1.1 *If* T *is a triangle in* $\mathbb{R}^3$ *then it is an affine image of the reference triangle:*

$$T = F(\hat{T}),$$

where $F : \mathbb{R}^2 \supset \hat{T} \ni \begin{bmatrix} \xi \\ \eta \end{bmatrix} \mapsto A \begin{bmatrix} \xi \\ \eta \end{bmatrix} + b \in T \subset \mathbb{R}^3$ *where* $A : \mathbb{R}^2 \to \mathbb{R}^3$ *is linear and* $b \in \mathbb{R}^3$*.*

The Lagrange's linear element (T, Π, Σ) is defined by: T is a planar triangle, $\Pi = \mathcal{P}_1(T)$ and the three functionals σ^i span Σ by $\sigma^i \in \Sigma \Leftrightarrow \sigma^i(f) = f(\mathbf{p}^i)$, where $\mathbf{p}^i$ is the coordinate vector of the ith vertex of the triangle.

The dual basis of $(\sigma^i)_i$ is denoted by $(\lambda^j)_{j=1}^3$, ie. it holds $\sigma^i(\lambda^j) = \delta_{ij}$. It turns out that $\Pi = span(\lambda^k)_{k=1}^3$.

One says that the Lagrange's linear basis function λ^i is associated with the jth vertex if $\sigma^j(\lambda^i) = 1$. A basis function λ^k is depicted in figure 1.1.

From implementation point of view, the basis functions are constructed the usual way from the reference element. The reference element is just a Lagrange's linear element for which $T = \hat{T}$. Each basis function is constructed by composition with affine mapping which maps the reference triangle $\hat{T}$ to T:

$$\lambda^i = \hat{\lambda}^i \circ F^{-1},$$

where $\hat{\lambda}^i : \hat{T} \to \mathbb{R}$ is defined by

$$\begin{aligned} \hat{\lambda}^1(\xi, \eta) &= 1 - \xi - \eta, \\ \hat{\lambda}^2(\xi, \eta) &= \xi \quad \text{and} \\ \hat{\lambda}^3(\xi, \eta) &= \eta. \end{aligned}$$

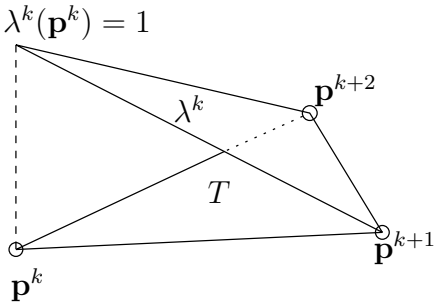

Figure 1.1: The graph of Lagrange's linear basis function λ^k on triangle T.

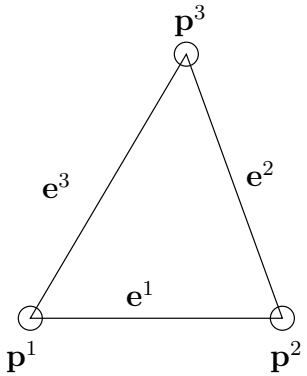

Figure 1.2: Local numbering on a triangle.

The Rao-Wilton-Glisson element [13] (T, Π, Σ) is defined by: T is a triangle, $\Pi = span(\mathbf{u}^i)_i$, where

$$\mathbf{u}^i(\mathbf{r}) := \frac{L^i}{2A}(\mathbf{r} - \mathbf{p}^{i+2}),$$

where L^i denotes the length of ith edge, A denotes the area of T and $\mathbf{p}^{i+2}$ denotes the coordinates to the opposing vertex to the edge i and $\Sigma = span(\sigma_i)_i$ where $\sigma_i(f)$ is the outer normal component of $f \in \Pi$ on edge i. Again $(\sigma_i)_i$ is the dual base of $(\mathbf{u}^i)_i$.

The local numbering of vertices $\mathbf{p}_i$ and edges $\mathbf{e}_i$ of triangle T is presented in figure 1.2.

The basis functions of Π of Rao-Wilton-Glisson (RWG) element can be also defined using basis functions of Lagrange's linear element:

$$\mathbf{r} - \mathbf{p}^{i+2} = (\mathbf{p}^i - \mathbf{p}^{i+2})\lambda^i(\mathbf{r}) + (\mathbf{p}^{i+1} - \mathbf{p}^{i+2})\lambda^{i+1}(\mathbf{r}), \tag{1.24}$$

where λ^i is associated with ith vertex. Thus the normal component of $\mathbf{u}^i$ to the triangle on the edge $\mathbf{e}^j$ is δ_{ij}.

The RWG-element can be seen as the Raviart-Thomas element [14] on a triangle embedded in $\mathbb{R}^3$.

1.6 Finite dimensional function spaces on polyhedrons

Let S be a surface of a polyhedron and let $\mathcal{T} = (T_m)_m$ be it's triangulation. Let RWG_m be the RWG-element which is associated with T_m, ie. $\mathrm{RWG}_m := (T_m, \Pi_m, \Sigma_m)$. Let T_m be adjacent triangle to T_n and $\mathbf{e}^i$ their shared edge. The shared edge is edge $\mathbf{e}^k$ in T_m and edge $\mathbf{e}^l$ in T_n. Thus the RWG-basis function on the polyhedron is defined as

$$\mathbf{u}_i = \begin{cases} \mathbf{u}_m^k, & \text{in } T_m \\ -\mathbf{u}_n^l, & \text{in } T_n \\ 0, & \text{elsewhere} \end{cases}, \tag{1.25}$$

where $\mathbf{u}_m^k$ is a basis function of RWG_m and $\mathbf{u}_n^l$ is a basis function of RWG_n. Although the basis functions are discontinuous on S, their normal component, wrt. edges of the triangles, is continuous over the edges and their surface divergence is an integrable function on S.

Heuristically speaking, the normal component continuity across edges is important as it ensures that no current is lost nor created at edges, ie. there are no current sources on edges.

The space spanned by RWG-basis functions on $\mathcal{T}$ is denoted by $\mathrm{RWG}(\mathcal{T})$.

Chapter 2

Scattering problems

The electromagnetic scattering problem considered in this thesis is posed as follows:

Problem 2.1 *Let D be a bounded open set with well-behaved boundary S. Let $\mathbf{E}_p$ and $\mathbf{H}_p$ be the primary fields of the source $(\mathbf{J}_p, \mathbf{M}_p)$ in homogeneous space. Let $(\mathbf{E}, \mathbf{H})$ be the solution to inhomogeneous Maxwell's equations where ε and μ are different constants in intD and extD.*

What are the scattered fields $\mathbf{E}_s$ *and* $\mathbf{H}_s$ *which satisfy*

$$\mathbf{E}_s = \mathbf{E} - \mathbf{E}_p \quad \text{and} \quad \mathbf{H}_s = \mathbf{H} - \mathbf{H}_p?$$

In the following the electric field, magnetic field and combined field integral equations (EFIE, MFIE and CFIE, respectively) are derived for perfectly electrically conducting scatterers. For dielectric scatterers, CFIE and Müller formulations are derived.

The open set D in the above problem is considered as the *scattering object*.

2.1 Derivation of the basic integral equations

Let ε_1, μ_1 and ε_2, μ_2, $Im(\varepsilon_1) < \infty$, be the constant electric permittivities and magnetic permeabilities in $extD$ and $intD$, respectively. Let $(\mathbf{E}, \mathbf{H})$ be the solution to Maxwell's equations with scattering object D and some given source. Let $\mathbf{E}_1 := \mathbf{E}_{|extD}$, $\mathbf{H}_1 := \mathbf{H}_{|extD}$, $\mathbf{E}_2 = \mathbf{E}_{|intD}$ and $\mathbf{H}_2 := \mathbf{H}_{|intD}$.

The boundary conditions for the fields read as

$$\hat{\mathbf{n}} \times \mathbf{E}_1 = \hat{\mathbf{n}} \times \mathbf{E}_2 \quad \text{and} \quad \hat{\mathbf{n}} \times \mathbf{H}_1 = \hat{\mathbf{n}} \times \mathbf{H}_2 \quad \text{on } S. \tag{2.1}$$

Let $\mathbf{E}_s$ and $\mathbf{H}_s$ be again such that $\mathbf{E}_1 = \mathbf{E}_s + \mathbf{E}_p$ and $\mathbf{H}_1 = \mathbf{H}_s + \mathbf{H}_p$ in $extD$, respectively. Thus $\mathbf{E}_s$ satisfies the exterior Stratton-Chu formula (1.17) and $\mathbf{H}_s$

satisfies the exterior Stratton-Chu formula (1.18) with $k = k_1 = \omega\sqrt{\epsilon_1\mu_1}$. Clearly $\mathbf{E}_p$ and $\mathbf{H}_p$ satisfy the interior Stratton-Chu formulas (1.15) and (1.16) with $k = k_1$.

Finally, $\mathbf{E}_2$ and $\mathbf{H}_2$ satisfy the interior Stratton-Chu equations (1.15) and (1.16), respectively, with $k = k_2 = \omega\sqrt{\varepsilon_2\mu_2}$. Recall that $Im(k) \geq 0$.

After some manipulations (see appendix A for details) one obtains the electric and magnetic field equations for D_1 and D_2:

$$-\frac{1}{i\omega\varepsilon_1}\tilde{D}_{k_1}(\mathbf{J}) - \tilde{K}_{k_1}(\mathbf{M}) + \frac{1}{2}\mathbf{M} = -\hat{\mathbf{n}} \times \mathbf{E}_p, \tag{2.2}$$

$$-\frac{1}{i\omega\mu_1}\tilde{D}_{k_1}(\mathbf{M}) + \tilde{K}_{k_1}(\mathbf{J}) - \frac{1}{2}\mathbf{J} = -\hat{\mathbf{n}} \times \mathbf{H}_p, \tag{2.3}$$

$$-\frac{1}{i\omega\varepsilon_2}\tilde{D}_{k_2}(\mathbf{J}) - \tilde{K}_{k_2}(\mathbf{M}) - \frac{1}{2}\mathbf{M} = 0 \text{ and} \tag{2.4}$$

$$-\frac{1}{i\omega\mu_2}\tilde{D}_{k_2}(\mathbf{M}) + \tilde{K}_{k_2}(\mathbf{J}) + \frac{1}{2}\mathbf{J} = 0 \tag{2.5}$$

in S. These equations are denoted by EFIE_1, MFIE_1, EFIE_2 and MFIE_2, respectively.

2.1.1 EFIE and MFIE formulations for PEC

Let D be a perfectly electrically conducting (PEC) object, ie. $Im(\varepsilon_2) = \infty$ in D. Then on $S = \partial D$ it holds

$$\hat{\mathbf{n}} \times \mathbf{E} = 0. \tag{2.6}$$

By noticing that $\mathbf{M} = -\hat{\mathbf{n}} \times \mathbf{E} = 0$ and inspecting equation (2.2) one obtains the EFIE formulation for PEC object:

$$\frac{1}{i\omega\varepsilon}\tilde{D}_k(\mathbf{J}) = \hat{\mathbf{n}} \times \mathbf{E}_p \quad \text{in } S. \tag{2.7}$$

This equation suffers from the fact that at interior resonances frequencies the $\tilde{D}_k$ fails to be injective, ie. (2.7) is not uniquely solvable and this property is inherited to numerical solution scheme causing the system[1] matrix to be singular.

This can be seen by considering the interior resonance problem. Supposing that the material parameters in $intD$ equal those of in $extD$. Then the sourceless Maxwell's equations in $intD$ with condition $\hat{\mathbf{n}} \times \mathbf{E} = 0$ on ∂D have non-trivial solutions. Thus

$$\frac{-1}{i\omega\varepsilon}(D_k(\mathbf{J})(\mathbf{r}) = -\mathbf{E}(\mathbf{r}), \quad \text{in } intD$$

by Stratton-Chu formula (1.15) so that $\mathbf{J}$ cannot be zero everywhere on ∂D, but by multiplying both sides with $\hat{\mathbf{n}}\times$ and taking limit from inside one obtains

$$\frac{-1}{i\omega\varepsilon}(\tilde{D}_k(\mathbf{J})(\mathbf{r}) = -\hat{\mathbf{n}} \times \mathbf{E}(\mathbf{r}) = 0, \quad \text{in } \partial D,$$

[1] definition of system matrix will be given in section 2.2

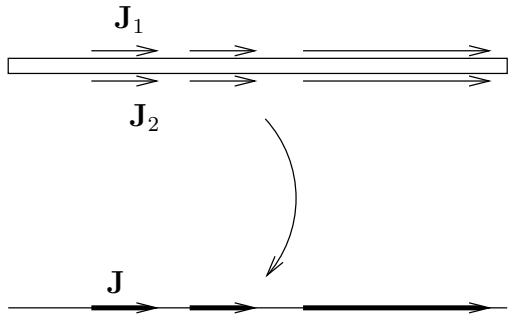

Figure 2.1: The generalisation of EFIE formulation to non-closed surfaces.

which is the desired result.

Another problem with EFIE formulation is that it behaves badly when Krylov[2] subspace iterative solvers, such as GMRES, are applied to its discretization. The condition number of the resulting system matrix will tend to ∞ as $\omega \to 0$ or when the element size tends to 0. Such phenomenon is called the *low-frequency breakdown* in the literature [15]. The low-frequency breakdown is problematic when one wishes to model scattering objects that have small details: just representing the object by triangulation will cause element size to become small.

The EFIE can be generalised to cover patch scatterers, ie. non-closed surfaces. The generalisation is done heuristically by considering an object with thickness but that which is very thin. The currents on both sides of the object are almost identical and thus the currents can be thought as if they were one single current. This generalisation is depicted in figure 2.1

The MFIE formulation can be derived in similar manner from the equation MFIE_1 (2.3) and applying the PEC boundary condition (2.6).

$$\tilde{K_k}(\mathbf{J}) - \frac{1}{2}\mathbf{J} = -\hat{\mathbf{n}} \times \mathbf{H}_p. \tag{2.8}$$

The MFIE formulation also suffers from loss of uniqueness of the solution at certain frequencies [8]. Comparing MFIE and EFIE numerically one observes that MFIE is less accurate than EFIE. Especially when the object has sharp edges, the solution by MFIE becomes less accurate.

On the other hand, MFIE does not suffer from low frequency breakdown and it has good iterative properties.

2.1.2 CFIE formulation

Combining EFIE and MFIE as

$$\alpha\,\text{EFIE} + (1-\alpha)\eta\hat{\mathbf{n}} \times \text{MFIE},$$

[2]Alexei Nikolaevich Krylov (1863-1945)

where $\eta = \sqrt{\mu/\varepsilon}$ and $\alpha \in [0,1]$, one obtains the so called combined field integral equation (CFIE) for a PEC-scatterer:

$$\alpha \frac{1}{i\omega\varepsilon}\tilde{D}_k(\mathbf{J}) + \eta(1-\alpha)\left[\hat{\mathbf{n}} \times \tilde{K}_k(\mathbf{J}) - \frac{1}{2}\hat{\mathbf{n}} \times \mathbf{J}\right] = \alpha\hat{\mathbf{n}} \times \mathbf{E}_p - \eta(1-\alpha)\hat{\mathbf{n}} \times \hat{\mathbf{n}} \times \mathbf{H}_p \tag{2.9}$$

This formulation has the advantage that for all $\omega > 0$ it has a unique solution [8]. The resulting system matrix has a much smaller condition number than pure the EFIE and the solution is more accurate than pure MFIE. The small condition number in turn guarantees a faster convergence of the GMRES iterations.

Similarly, for dielectric objects with $Im(\varepsilon_2) < \infty$, one can combine EFIE_i and MFIE_i to obtain different combined formulations.

The following combination is called CFIE formulation for dielectric object:

$$\begin{cases} \alpha\text{EFIE}_1 + (1-\alpha)\eta\hat{\mathbf{n}} \times \text{MFIE}_1 \\ \alpha\text{EFIE}_2 + (1-\alpha)\eta\hat{\mathbf{n}} \times \text{MFIE}_2 \end{cases}.$$

Or, in matrix-vector notation,

$$\mathcal{C}\begin{bmatrix} \mathbf{J} \\ \mathbf{M} \end{bmatrix} = \begin{bmatrix} -\alpha\hat{\mathbf{n}} \times \mathbf{E}_p - (1-\alpha)\eta\hat{\mathbf{n}} \times \hat{\mathbf{n}} \times \mathbf{H}_p \\ 0 \end{bmatrix}, \tag{2.10}$$

where $\mathcal{C}$ is defined by

$$\mathcal{C} = \begin{bmatrix} -\frac{\alpha}{i\omega\varepsilon_1}\tilde{D}_{k_1} + (1-\alpha)\eta\hat{\mathbf{n}} \times \left(\tilde{K}_{k_1} - \frac{1}{2}\right) & -\eta\frac{1-\alpha}{i\omega\mu_1}\hat{\mathbf{n}} \times \tilde{D}_{k_1} - \alpha\left(\tilde{K}_{k_1} + \frac{1}{2}\right) \\ -\frac{\alpha}{i\omega\varepsilon_2}\tilde{D}_{k_2} + (1-\alpha)\eta\hat{\mathbf{n}} \times \left(\tilde{K}_{k_2} + \frac{1}{2}\right) & -\eta\frac{1-\alpha}{i\omega\mu_2}\hat{\mathbf{n}} \times \tilde{D}_{k_2} - \alpha\left(\tilde{K}_{k_2} + \frac{1}{2}\right) \end{bmatrix}.$$

By a closer inspection one observes that when the PEC boundary condition (2.6) is applied, the resulting equation is the CFIE PEC when considering only the first row.

2.1.3 Müller formulation

The Müller formulation is defined for dielectric objects.

Let α_i and β_i, for $i = 1, 2$ be defined by

$$\alpha_i = \frac{2\mu_i}{\mu_1 + \mu_2} \quad \text{and} \quad \beta_1 = \frac{2\varepsilon_i}{\varepsilon_1 + \varepsilon_2}.$$

The Müller formulation then is defined by

$$\begin{cases} -\alpha_1\text{MFIE}_1 + \alpha_2\text{MFIE}_2 \\ \beta_1\text{EFIE}_1 - \beta_2\text{EFIE}_2 \end{cases}$$

or, in matrix-vector notation,

$$\mathcal{M} \begin{bmatrix} \mathbf{J} \\ \mathbf{M} \end{bmatrix} = \begin{bmatrix} \alpha_1 \hat{\mathbf{n}} \times \mathbf{H}_p \\ -\beta_1 \hat{\mathbf{n}} \times \mathbf{E}_p \end{bmatrix}, \tag{2.11}$$

where $\mathcal{M}$ is defined by

$$\mathcal{M} = \begin{bmatrix} \frac{2}{\mu_1+\mu_2}\left[\mu_2 \tilde{K}_{k_2} - \mu_1 \tilde{K}_{k_1}\right] + I & \frac{2}{i\omega(\mu_1+\mu_2)}\left[\tilde{D}_{k_1} - \tilde{D}_{k_2}\right] \\ \frac{2}{i\omega(\varepsilon_1+\varepsilon_2)}\left[\tilde{D}_{k_2} - \tilde{D}_{k_1}\right] & \frac{2}{\varepsilon_1+\varepsilon_2}\left[\varepsilon_2 \tilde{K}_{k_2} - \varepsilon_1 \tilde{K}_{k_1}\right] + I \end{bmatrix}. \tag{2.12}$$

The kernel of $\tilde{D}_{k_1} - \tilde{D}_{k_2}$ is weakly singular [15]. This fact simplifies the numerical treatment as no differentiability restrictions need to be posed on basis nor test functions.

In addition, the Müller formulation has the following desirable properties. It does not suffer from loss of uniqueness of the solution at any frequencies [8] and it has very good low frequency properties [16]. The convergence is studied in section 2.3 in more detail.

2.2 Discretization

Let D be a polyhedron and $\mathcal{T}$ be a triangulation on the boundary S of D. The numerical solutions of the scattering problem 2.1 are based on the integral equations (2.7), (2.8), (2.9), (2.10) and (2.11).

The discrete counterpart of these equations are derived by means of projection onto $V = \mathrm{RWG}(\mathcal{T})$ or $V = \hat{\mathbf{n}} \times \mathrm{RWG}(\mathcal{T})$.

Let A be the integral operator acting on fields on S and let f be in the range of A. Let $U_{\mathcal{T}} = \mathrm{RWG}(\mathcal{T})$ or $U_{\mathcal{T}} = \mathrm{RWG}(\mathcal{T})$ and $V = \mathrm{RWG}(\mathcal{T})$ or $V = \hat{\mathbf{n}} \times \mathrm{RWG}(\mathcal{T})$. Let P be an orthogonal projection wrt. $\langle \cdot, \cdot \rangle$ of certain tangential fields on S onto $V_{\mathcal{T}}$.

The discrete equation now takes the form

$$PAx = Pf, \quad x \in U_{\mathcal{T}}, \tag{2.13}$$

which is equivalent with

$$\langle y, Ax \rangle = \langle y, f \rangle \quad \forall y \in V_{\mathcal{T}}. \tag{2.14}$$

This is just a system of linear equations

$$\mathbf{Ax} = \mathbf{f}$$

and for a small dimension of the space $\mathrm{RWG}(\mathcal{T})$ it can be solved, for example, by the LU-factorisation. Krylov-subspace methods, such as the GMRES iteration, would come into consideration if their convergence were fast enough.

The matrix $\mathbf{A}$ is called the *system matrix* of the problem (2.14).

The functions in $V_{\mathcal{T}}$ are called test functions and the functions in $U_{\mathcal{T}}$ are called basis functions.

The choices of test and basis function spaces must be carefully selected for different formulations. In table 2.1 the feasible test and basis function spaces are collected for different formulations. For justification see [8], [16].

Table 2.1: Feasible choices for test and basis function spaces for different formulations

Formulation	Test functions	Basis functions
EFIE PEC	$\hat{\mathbf{n}} \times$ RWG	RWG
MFIE PEC	RWG	RWG
CFIE PEC	$\hat{\mathbf{n}} \times$ RWG	RWG
Müller	RWG	RWG

Recall that the RWG-basis functions are denoted by $\mathbf{u}_m$ ie. $\mathrm{RWG}(\mathcal{T}) = span(\mathbf{u}_m)_{m=1}^N$.

The discrete form of EFIE for PEC scatterer (2.7) reads as

$$\frac{1}{i\omega\varepsilon}\left\langle \hat{\mathbf{n}} \times \mathbf{u}_m, \tilde{D}_k\left(\sum_{n=1}^{N} x_n \mathbf{u}_n\right)\right\rangle = \langle \hat{\mathbf{n}} \times \mathbf{u}_m, \hat{\mathbf{n}} \times \mathbf{E}_p\rangle \quad \forall m = 1 \ldots N, x_n \in \mathbb{C}. \tag{2.15}$$

This equation is to be modified in order to efficiently calculate the elements

$$\left\langle \hat{\mathbf{n}} \times \mathbf{u}_m, \frac{1}{i\omega\varepsilon}\tilde{D}_k(\mathbf{u}_n)\right\rangle$$

of the system matrix. The first term of the sesquilinear form $\langle \cdot, \cdot \rangle$ was complex-conjugated but the conjugation symbol may be omitted since $\hat{\mathbf{n}} \times \mathbf{u}_m$ is real. Thus writing the sesquilinear form above open yields

$$\frac{1}{i\omega\varepsilon}\int_S \hat{\mathbf{n}}(\mathbf{r}) \times \mathbf{u}_m(\mathbf{r}) \cdot \int_S \hat{\mathbf{n}}(\mathbf{r}) \times (\nabla\nabla\cdot + k^2) g_k(\mathbf{r}, \mathbf{r}')\mathbf{u}_n(\mathbf{r}')d\mathbf{r}'d\mathbf{r}.$$

By taking the $\hat{\mathbf{n}}\times$ out from the inner integral and using the vector identity

$$a \cdot b \times c = a \times b \cdot c$$

and the fact that since $\mathbf{u}_m(\mathbf{r})$ is orthogonal to $\hat{\mathbf{n}}(\mathbf{r})$ it holds

$$(\hat{\mathbf{n}}(\mathbf{r}) \times \mathbf{u}_m(\mathbf{r})) \times \hat{\mathbf{n}}(\mathbf{r}) = \mathbf{u}_m(\mathbf{r}),$$

and thus

$$\frac{1}{i\omega\varepsilon}\left\langle \hat{\mathbf{n}} \times \mathbf{u}_m, \tilde{D}_k(\mathbf{u}_n)\right\rangle = \frac{1}{i\omega\varepsilon}\int_S \mathbf{u}_m(\mathbf{r}) \cdot \int_S (\nabla\nabla\cdot + k^2) g_k(\mathbf{r}, \mathbf{r}')\mathbf{u}_n(\mathbf{r}')d\mathbf{r}'d\mathbf{r}$$

holds.

The right hand side of the above equation naturally decouples into two expressions: One expression that has $\nabla\nabla\cdot$ in it and one that has k^2 in it. The expression that has $\nabla\nabla\cdot$ in it is then manipulated in the following way:

$$\begin{aligned}\int_S \mathbf{u}_m \cdot \nabla \int_S \nabla \cdot (g_k \mathbf{u}_n) d\mathbf{r} &= \\ -\int_S \nabla \cdot \mathbf{u}_m \int_S \nabla \cdot (g_k \mathbf{u}_n) d\mathbf{r}' d\mathbf{r} &= \\ -\int_S \nabla \cdot \mathbf{u}_m \int_s g_k \nabla' \cdot \mathbf{u}_n d\mathbf{r}' d\mathbf{r}.&\end{aligned}$$

Here in the first equation the gradient is moved to divergence by integration by parts. In the second equation, the following identity is used:

$$\nabla g_k = -\nabla' g_k,$$

where ∇' denotes the derivative with respect to $\mathbf{r}'$. Thus the gradient of the Green's function can be moved to divergence of the basis function by integration by parts. Note that divergences applied to $\mathbf{u}_m$ and $\mathbf{u}_n$ are considered as surface divergences.

Remark 2.1 *The integration by parts does not produce boundary integral terms when test functions are in $RWG(\mathcal{T})$ for they have continuous normal component over the edges.*

Similarly, it holds

$$\int_S \hat{\mathbf{n}} \times \mathbf{u}_m \cdot k^2 \int_S \hat{\mathbf{n}} \times g_k \mathbf{u}_n d\mathbf{r}' d\mathbf{r} = \int_s \mathbf{u}_m \cdot \int_s g_k \mathbf{u}_n d\mathbf{r}' d\mathbf{r}.$$

Collecting the results one obtains the formula to calculate the elements of the system matrix $\mathbf{A}$:

$$\mathbf{A}_{mn} = \frac{i}{\omega\varepsilon} \int_S \nabla \cdot \mathbf{u}_m \int_S g_k \nabla' \cdot \mathbf{u}_n d\mathbf{r}' d\mathbf{r} - i\omega\mu \int_S \mathbf{u}_m \cdot \int_S g_k \mathbf{u}_n d\mathbf{r}' d\mathbf{r}. \tag{2.16}$$

This is not, however, yet the recipe to assemble the system matrix. Instead one calculates the so called *local system matrices*

$$\mathbf{A}_{mn}^{pq} = \frac{i}{\omega\varepsilon} \int_{T_m} \nabla \cdot \mathbf{u}_m^p \int_{T_n} g_k \nabla' \cdot \mathbf{u}_n^q d\mathbf{r}' d\mathbf{r} - i\omega\mu \int_{T_m} \mathbf{u}_m^p \cdot \int_{T_n} g_k \mathbf{u}_n^q d\mathbf{r}' d\mathbf{r}$$

and adds these to right places in the system matrix. Here $p, q \in \{1, 2, 3\}$ and thus $\mathbf{A}_{mn}^{pq}$ is a 3×3 matrix wrt. p and q. Recall that $\mathbf{u}_m^p$:s denote the basis functions of element T_m.

Remark 2.2 *The restrictions of global basis functions on elements are the local basis functions multiplied by* -1 *or* 1 *as stated in equation (1.25).*

Recalling that

$$\mathbf{u}_m^p = \frac{L_m^p}{A_m}\left((\mathbf{p}_m^p - \mathbf{p}_m^{p+2})\lambda_m^p + (\mathbf{p}_m^{p+1} - \mathbf{p}_m^{p+2})\lambda_m^{p+1}\right)$$

holds and by noticing that $\mathbf{p}_m^p$ is constant for each $p \in \{1,2,3\}$ one sees that only integrals

$$\mathbf{I}_{mn}^{pq} = \int_{T_m} \lambda_m^p(\mathbf{r}) \int_{T_n} g_k(\mathbf{r},\mathbf{r}')\lambda_n^q(\mathbf{r}')d\mathbf{r}'d\mathbf{r}$$

are required to calculate the system matrix of the discrete EFIE formulation.

For the MFIE PEC formulation the local system matrix entries $\mathbf{B}_{mn}^{pq}$ are defined by

$$\mathbf{B}_{mn}^{pq} = \int_{T_m} \mathbf{u}_m^p \cdot \hat{\mathbf{n}} \times \int_{T_n} \nabla \times (g_k \mathbf{u}_n^q) d\mathbf{r}'d\mathbf{r},$$

which is equivalent with

$$\mathbf{B}_{mn}^{pq} = \int_{T_m} \mathbf{u}_m^p \times \hat{\mathbf{n}} \cdot \int_{T_n} \nabla g_k \times \mathbf{u}_n^q d\mathbf{r}'d\mathbf{r}$$

after some manipulations.

In the case of Müller formulation, this is not yet enough, since the testing is done with RWG functions and thus one needs to calculate integrals of type

$$\begin{aligned}
\mathbf{D}_{mn} &= \int_S \mathbf{u}_m(\mathbf{r}) \cdot \hat{\mathbf{n}} \times \int_S \nabla\nabla \cdot (g_k(\mathbf{r},\mathbf{r}')\mathbf{u}_n(\mathbf{r}'))d\mathbf{r}'d\mathbf{r} \\
&= \sum_{p,q} \int_{T_p} u_m(\mathbf{r})\hat{\mathbf{n}}(\mathbf{r}) \cdot \nabla \int_{T_q} \nabla \cdot g_k(\mathbf{r},\mathbf{r}')\mathbf{u}_n(\mathbf{r}')d\mathbf{r}'d\mathbf{r} \\
&= \sum_{p,q} \int_{T_p} \nabla \cdot \left[\mathbf{u}_m(\mathbf{r}) \times \hat{\mathbf{n}}(\mathbf{r}) \int_{T_q} \nabla \cdot g(\mathbf{r},\mathbf{r}')\mathbf{u}_n(\mathbf{r}')d\mathbf{r}'\right] d\mathbf{r} \\
&= \sum_{p,q} \int_{\partial T_p} \nu_p(\mathbf{r}) \cdot \mathbf{u}_m(\mathbf{r}) \times \hat{\mathbf{n}}(\mathbf{r}) \int_{T_q} g_k(\mathbf{r},\mathbf{r}')\nabla' \cdot \mathbf{u}_n(\mathbf{r}')d\mathbf{r}'d\mathbf{r}.
\end{aligned}$$

As with EFIE formulation, the integrals are calculated using the Lagrange's local basis functions.

To calculate $\mathbf{B}_{mn}^{pq}$ using Lagrange's local basis functions one must pay attention to the gradient of the Green's function. Writing the gradient in local coordinates and using the following formula:

$$\nabla g(\mathbf{r},\mathbf{r}') \times \mathbf{f} = -\frac{\partial g(\mathbf{r},\mathbf{r}')}{\partial \hat{\mathbf{n}}'}\hat{\mathbf{n}} \times \mathbf{f} + \hat{\mathbf{n}}\left(\nabla'_S g(\mathbf{r},\mathbf{r}') \cdot \hat{\mathbf{n}} \times \mathbf{f}\right), \quad \text{if } \hat{\mathbf{n}} \cdot \mathbf{f} = 0,$$

the local system matrix $\mathbf{B}_{mn}^{pq}$ can be written as

$$\mathbf{B}_{mn}^{pq} = \int_{T_m} \mathbf{u}_m^p \times \hat{\mathbf{n}} \cdot \left(\int_{T_n} -\frac{\partial g}{\partial \hat{\mathbf{n}}'} \hat{\mathbf{n}}' \times \mathbf{u}_n^q d\mathbf{r}' + \int_{T_n} \hat{\mathbf{n}}' (\nabla_S' g \cdot \hat{\mathbf{n}}' \times \mathbf{u}_n^q) d\mathbf{r}' \right) d\mathbf{r}.$$

Finally, using Gauss's theorem and product rule of derivative, one obtains

$$\begin{aligned} \mathbf{B}_{mn}^{pq} = \int_{T_m} \hat{\mathbf{n}} \times \mathbf{u}_m^p \cdot \int_{T_n} \frac{\partial g}{\partial \hat{\mathbf{n}}'} \hat{\mathbf{n}}' \times \mathbf{u}_n^q d\mathbf{r}' d\mathbf{r} - \\ \int_{\partial T_n} \hat{\mathbf{n}}' \times \mathbf{u}_n^p \cdot \nu' \int_{T_m} g \hat{\mathbf{n}} \times \mathbf{u}_m^q \cdot \hat{\mathbf{n}}' d\mathbf{r} d\mathbf{r}'. \end{aligned} \tag{2.17}$$

From this one sees that to calculate the MFIE system matrix one only needs to calculate the following integrals

$$\mathbf{J}_{mn}^{ij} = \int_{T_m} \lambda_m^i \int_{T_n} \frac{\partial g}{\partial \hat{\mathbf{n}}} \lambda_n^j d\mathbf{r}' d\mathbf{r},$$

$$\mathbf{K}_{mn}^{ij} = \int_{\partial T_n} \lambda_n^j \int_{T_m} g \lambda_m^i d\mathbf{r}' d\mathbf{r} \quad \text{and}$$

$$\mathbf{id}_{mn}^{ij} = \int_{T_m \cap T_n} \lambda_m^i \lambda_n^j d\mathbf{r}.$$

And it turns out, that these, in addition to $\mathbf{I}_{mn}^{pq}$, are the only integrals needed to calculate the system matrix for Müller and CFIE formulations.

In the calculation of $\mathbf{I}_{mn}^{pq}$, $\mathbf{J}_{mn}^{pq}$ and $\mathbf{K}_{mn}^{pq}$ by numerical quadrature one has to calculate integrals of type

$$\int g(\mathbf{r}, \mathbf{r}') \lambda^q(\mathbf{r}') d\mathbf{r}',$$

which are tediously hard to calculate using only numerical quadrature. Therefore, they are calculated using the *singularity subtraction technique*:

The Green's function $g_k(\mathbf{r}, \mathbf{r}')$ has a series expansion due to Laurent's series of the function e^{iz}/z:

$$g_k(\mathbf{r}, \mathbf{r}') = \frac{1}{4\pi} \sum_{n=0}^{\infty} \frac{(ik)^n \, ||\mathbf{r} - \mathbf{r}'||^{n-1}}{n!}.$$

And the first few terms of this series is integrated analytically. The tail series converges to a function that is everywhere continuous and bounded in compact sets and thus it can be efficiently integrated numerically by using Gaussian quadrature. For the derivation of such analytical formulas, see [4], [3].

2.2.1 On implementation

There are three main data structures that are used in the implementation:

Nodes is a $(3, M)$-table containing the nodal data given by

$$\texttt{nodes(:,i)} = \mathbf{p}_i = \begin{bmatrix} p_{1i} \\ p_{2i} \\ p_{3i} \end{bmatrix},$$

where $\mathbf{p}_i$ is the ith node and p_{ji} is it's jth coordinate. Here MATLAB notation is used: `nodes(:,i)` denotes the ith column of `nodes` table.

Elements is a $(6, N)$-table containing the element data. Element T_i is given by

$$\texttt{elements(:,i)} = \mathbf{t}_i = \begin{bmatrix} n_{1i} \\ n_{2i} \\ n_{3i} \\ s_{1i}e_{1i} \\ s_{2i}e_{2i} \\ s_{3i}e_{3i} \end{bmatrix},$$

where $n_{ji} \in \mathbb{N}$ is the global nodal index of the jth vertex of the ith element, $e_{ji} \in \mathbb{N}$ is the global index of the jth edge of ith element and $s_{ji} \in \{-1, 1\}$ denotes whether local orientation of jth edge in the element is consistent with global orientation given by edge data. It is required that each $s_{ij}e_{ij} \in \mathbb{Z}$ is in the element data only once. This will make the construction of global basis functions from local basis functions easy: $\mathbf{u}_{e_{in}} = s_{in}\mathbf{u}_n^i$ in T_n.

Edges is a $(3, R)$ table containing the edge data. Edge i is given by

$$\texttt{edges(:,i)} = \mathbf{e}_i = \begin{bmatrix} n_{1i} \\ n_{2i} \\ s_i \end{bmatrix},$$

where $n_{ji} \in \mathbb{N}$ is jth node of ith edge and $s_i = 1$ if the edge $\mathbf{e}_i$ is on the boundary and $s_i = 0$ if not.

Let $\mathbf{A}_{mn}^{pq}$ be the local system matrix of the used formulation. Suppose additionally that

$$\mathbf{A}_{mn}^{pq} = \mathbf{A}_{nm}^{qp}. \tag{2.18}$$

Then, using data structures above, the system matrix assembly routine is as follows:

$\mathbf{A} \leftarrow \mathbf{0}$;
foreach $m, n = 1 \ldots N,\ n \leq m$ **do**
  foreach $p, q \in \{1, 2, 3\}$ **do**
    $r \leftarrow abs(\texttt{elements}(\texttt{p} + 3, \texttt{m}))$;
    $s \leftarrow abs(\texttt{elements}(\texttt{q} + 3, \texttt{n}))$;
    $\hat{r} \leftarrow sign(\texttt{elements}(\texttt{p} + 3, \texttt{m}))$;
    $\hat{s} \leftarrow sign(\texttt{elements}(\texttt{q} + 3, \texttt{n}))$;
    $\mathbf{A}(r, s) \leftarrow \mathbf{A}(r, s) + \mathbf{A}_{mn}^{pq} \hat{r}\hat{s}$;
    if $m \neq n$ **then**
      $\mathbf{A}(s, r) \leftarrow \mathbf{A}(s, r) + \mathbf{A}_{mn}^{qp} \hat{s}\hat{r}$;
    end
  end
end

This algorithm is easy to modify if the local system matrices do not have the property (2.18). The local system matrices of EFIE PEC formulation do have this property.

The `nodes` table is used to calculate the integrals in local system matrices and the `edges` table is used in the visualisation.

Having these three data structures the structure of the solver can be divided in to five levels:

1. Exact integration of integrals of type
$$\int \frac{1}{||\mathbf{r} - \mathbf{r}'||^n} \lambda_q(\mathbf{r}') d\mathbf{r}'.$$
2. Integration of the integrals over triangles involving Lagrange's local basis functions using Gaussian quadrature.
3. Assembly of local system matrices.
4. (a) Assembly of global system matrix.
   (b) Mesh preprocessing.
   (c) Visualisation routines.
5. Solution of the system matrix equation and calculation of wanted field values.

Here the parts 1,2,3 and 4(a) are critical speed-wise and were to be written in C language to achieve reasonable system matrix assembly speeds.

2.3 The numerical study

In this section the properties of EFIE, MFIE, CFIE and Müller formulations are studied numerically. The properties are studied by scattering problem stated above with varying scatterer geometries and source frequencies.

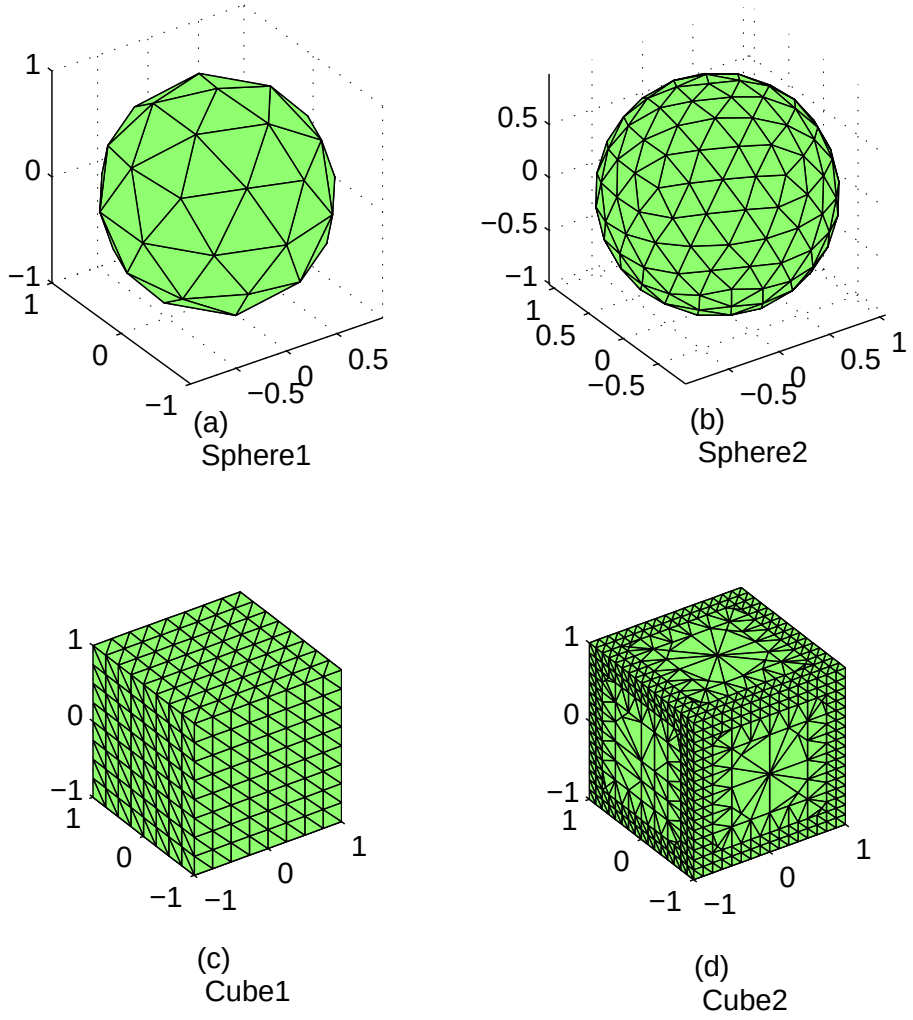

Figure 2.2: Used meshes to test scattering. They correspond to systems with 120, 480, 288 and 2892 DOFs from (a) to (d), respectively.

In the case of a spherical scatterer, the field solution obtained by the Mie series method is also presented. The Mie series calculations were performed using codes done by Jukka Sarvas and Henrik Kettunen and which were part of a package developed in electromagnetics laboratory. For overview of the Mie series method, see [17]. The sphere is approximated by a spherified subdivision icosahedron with 80 or 320 faces. Such meshes correspond to systems with 120 or 480 degrees of freedom (DOF), respectively. The used meshes are shown in figure 2.2. The sphere meshes were scaled to have the volume that of a sphere with radius of 1.

In each case, the x component of the real part of the scattered field is examined on

a circle in $\mathbb{R}^3$ parametrised by

$$C(t) = 10\,[0, \cos t, \sin t]\,, \quad -\pi < t < \pi.$$

The source is an electric dipole defined by $\mathbf{J}_d(\mathbf{r}) = \delta_{\mathbf{p}_d}(\mathbf{r})\mathbf{P}_d$, where $\mathbf{p}_d = [0, 60, -40]$ and $\mathbf{P}_d = [1, 0, 0]$. The scatterer is some object located at origin within a ball of radius of 10 m.

For PEC sphere with 120 DOFs EFIE, MFIE and CFIE perform equally well when the frequency is not an interior resonance frequency. The α parameter for CFIE is chosen to be $\frac{1}{2}$. The scattered field by EFIE, MFIE and CFIE is presented in figure 2.3.

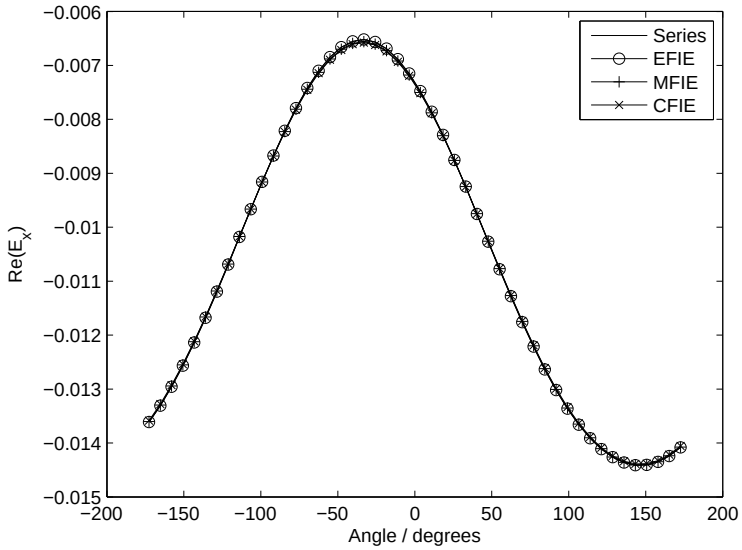

Figure 2.3: Scattered field comparison of due to the series, EFIE, MFIE and CFIE methods. Scattering mesh is the Sphere1.

If the scatterer contains sharp edges the precision of MFIE method deteriorates. This phenomenon can be seen by comparing the scattered field calculated with EFIE and MFIE due to parametrically deformed cube and the phenomenon is illustrated in figure 2.4. The calculations were performed on meshes Cube1 and Cube2.

The parametric deformation is defined by the mapping $\lambda : \mathbb{R}^3\backslash\{0\} \times \mathbb{R}^+ \to \mathbb{R}^3$

$$\lambda : (\mathbf{p}, t) \mapsto (1-t)\mathbf{p} + t\frac{\mathbf{p}}{||\mathbf{p}||}.$$

It holds that $\lambda(\cdot, 0) = \mathrm{id}$ and $\lambda(\cdot, 1)$ maps every point in it's domain to unit sphere.

The resonance frequencies of square PEC cavity with edge length of 2m can be calculated analytically. They are

$$f_{mnl} = \frac{\sqrt{(m\frac{1}{2}\pi)^2 + (n\frac{1}{2}\pi)^2 + (l\frac{1}{2}\pi)^2}}{2\pi\sqrt{\mu\varepsilon}}.$$

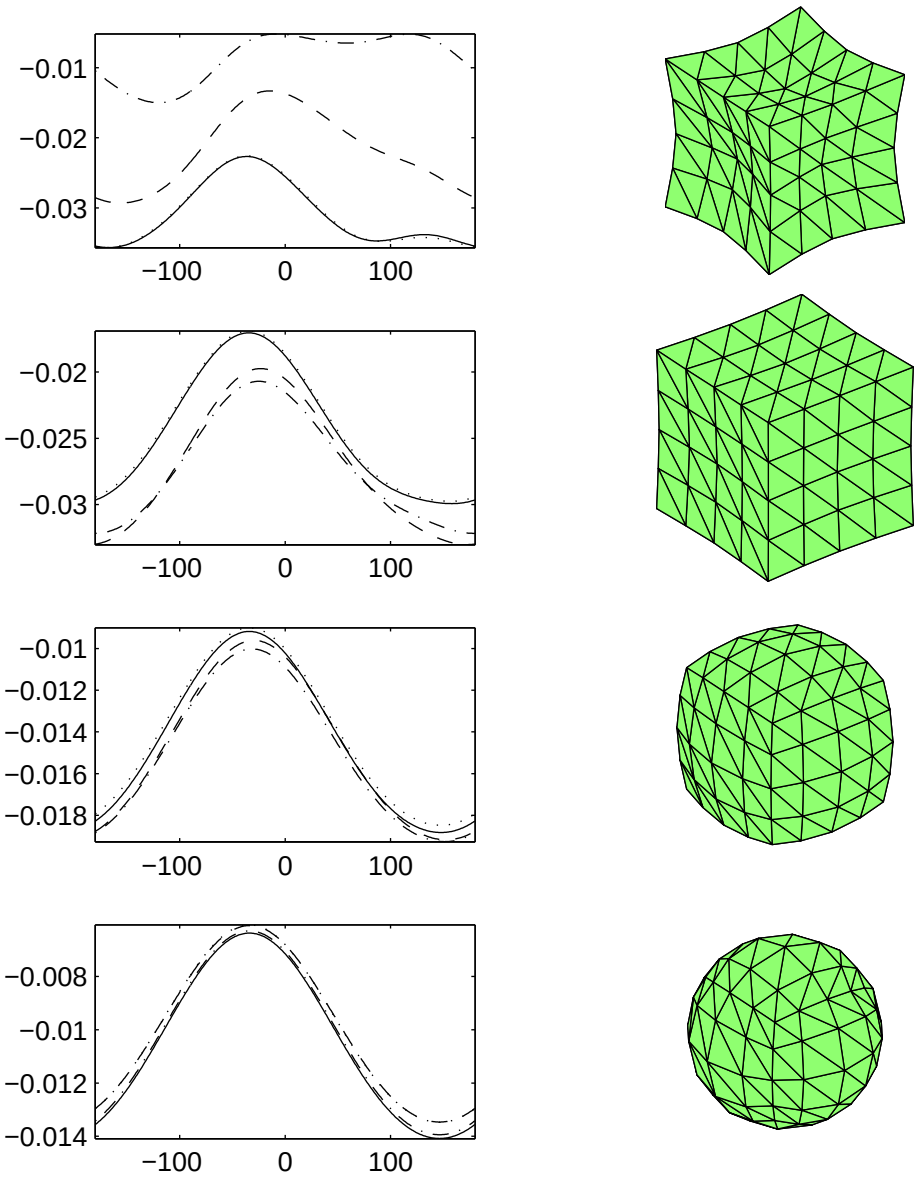

Figure 2.4: Scattered field due to a deformed cube. The scattered field on the plots correspond to the scatterer geometry depicted on the right side. Continuous line is the field due to EFIE from Cube2, dotted is due to EFIE from Cube1, dashed is due to MFIE from Cube1 and dash-dotted is due to MFIE from Cube2.

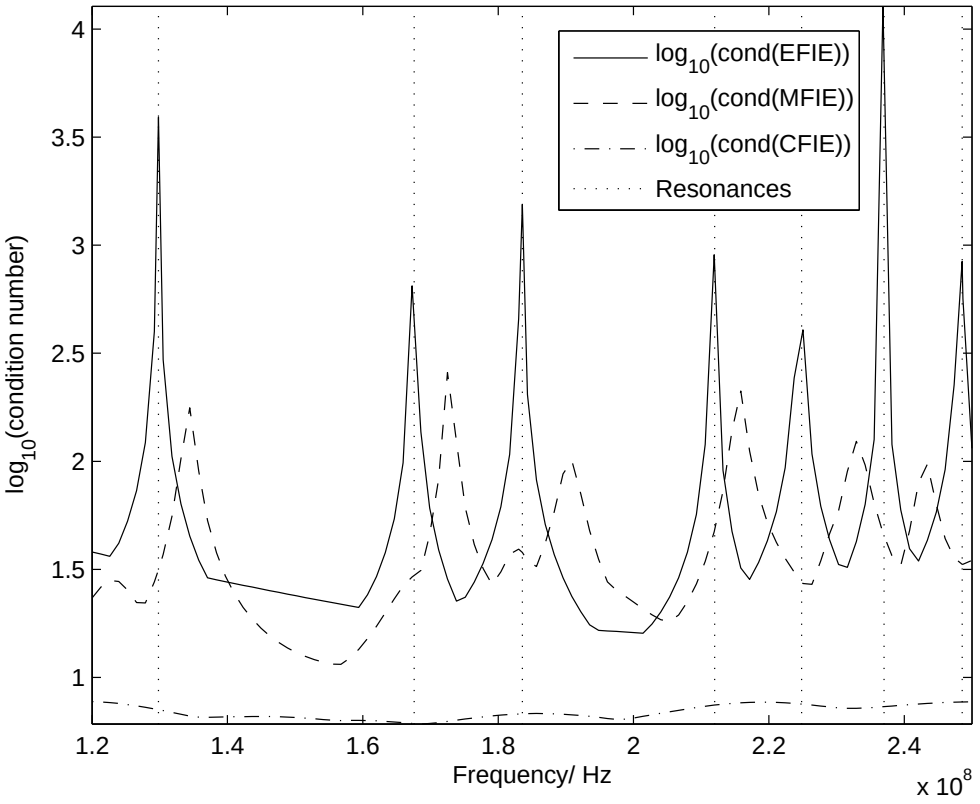

Figure 2.5: Condition number versus frequency of MFIE, EFIE and CFIE system matrices due to cube. The resonances are calculated analytically. The mesh is the Cube2.

Respectively, the resonance wave numbers k of spherical PEC cavity are obtained [18] by the solutions of

$$j_n(ka) = 0 \quad \text{or} \quad \frac{\partial}{\partial x}(xj_n(x)))_{|x=ka} = 0,$$

where a is the radius of the sphere and j_n is the spherical Bessel function of index n.

Plotting the condition number of the system matrix of the EFIE formulation reveals spikes at the resonance frequencies as seen in figures 2.5 and 2.6. This behaviour can be explained by noticing that the operator $\tilde{D}_k$ fails to be injective at the interior resonance frequencies and thus one should expect the system matrix of the discretized EFIE to become nearly singular.

One should also notice that in the figures 2.5 and 2.6 the condition number of the MFIE system matrix also has spikes, but the CFIE system matrix has excellent condition number throughout the sweep. This remark gives rise to conjecture

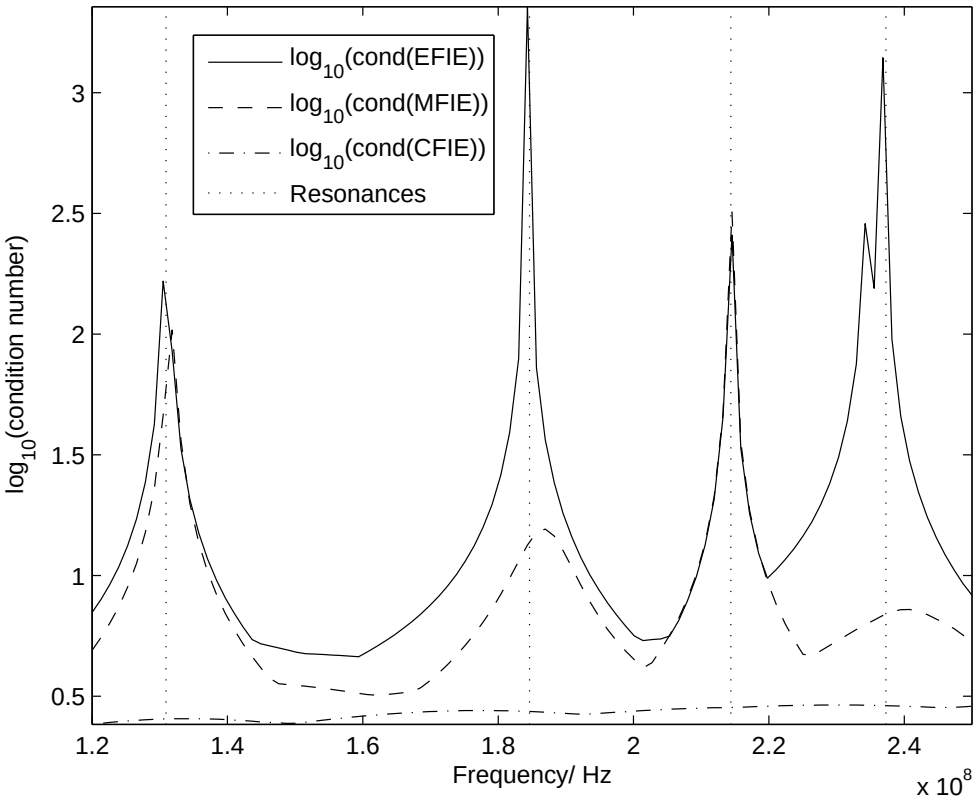

Figure 2.6: Condition number versus frequency of MFIE, EFIE and CFIE system matrices due to sphere. The resonances are calculated analytically. The mesh is the Sphere2.

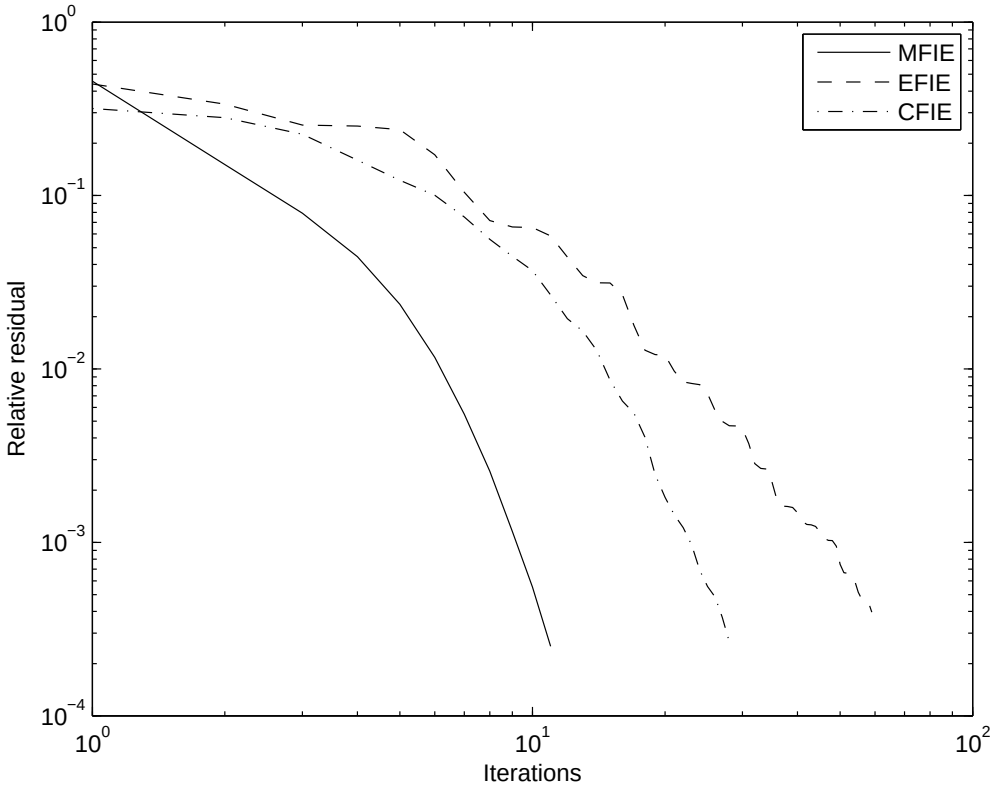

Figure 2.7: The GMRES convergence curves of EFIE, MFIE and CFIE formulations. The iteration stopping tolerance is 10^{-3}.

"$\ker\{\tilde{D}_k\} \cap \ker\{\tilde{K}_k - \frac{1}{2}\mathrm{id}\} = \{0\}$". Notice that this is vaguely posed since the space on which $\tilde{D}_k$ and $\tilde{K}_k - \frac{1}{2}\mathrm{id}$ operate is not defined.

Upon solving the discrete scattering equation (at frequency $f = 30\,\mathrm{MHz}$) iteratively using GMRES iteration with stopping tolerance 10^{-3} and iteration restart value 20, the convergence curves of EFIE, MFIE and CFIE formulations are depicted in figure (2.7). The MFIE required 10, CFIE required 27 and EFIE required 78 iterations to reach the tolerance.

The *low-frequency breakdown* is seen by inspecting the condition number of the EFIE, MFIE and CFIE system matrices. The condition number of EFIE system matrix is much higher than that of CFIE. For MFIE, there is no low-frequency breakdown. This phenomenon is illustrated for sphere in figure 2.8.

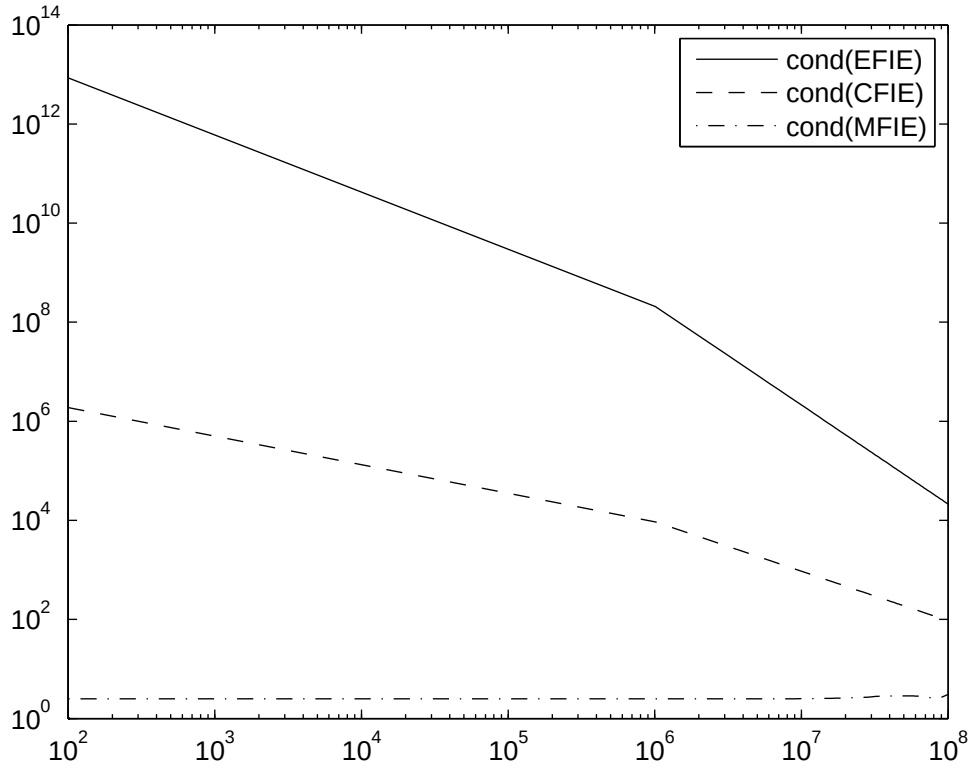

Figure 2.8: The condition number of EFIE and CFIE grows fast when the frequency tends to zero. Notice that the condition number of MFIE stays very small.

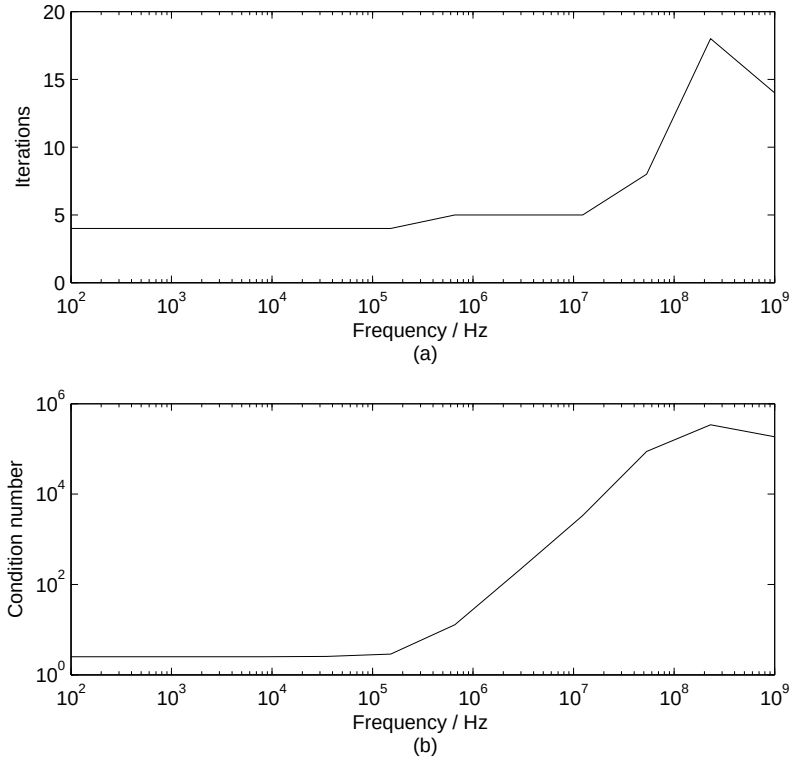

Figure 2.9: Solving iteratively the system matrix equation of Müller formulation using GMRES. (a) The number of required iterations at different frequencies. (b) The condition number of system matrix.

In the case of a dielectric scatterer, the Müller formulation is studied numerically. In the figures 2.11 (a-d) it is seen that the Müller formulation produces almost the same solution as the Mie series method and that the relative error stays approximately constant for different values of ε.

The Müller formulation has good convergence properties at wide range of frequencies as seen in figure 2.9. The high condition number at high frequencies doesn't cause the GMRES iteration to become unusable as at frequencies above $30 \cdot 10^8 Hz$ the discretization is too coarse for real calculations. The wavelength at this frequency is about 0.1 m and the average edge length is about 0.78 m. The used mesh was Sphere1. The GMRES stopping tolerance for relative residual was 10^{-3}. The convergence curves for frequencies $30 \cdot 10^3$, $30 \cdot 10^5$ and $30 \cdot 10^7$ Hz are presented in figure 2.10.

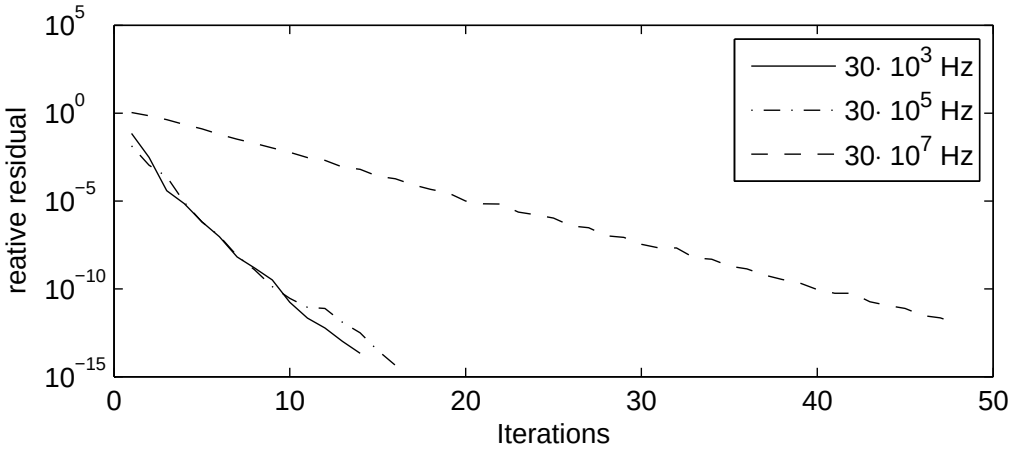

Figure 2.10: GMRES convergence curve for three different frequencies.

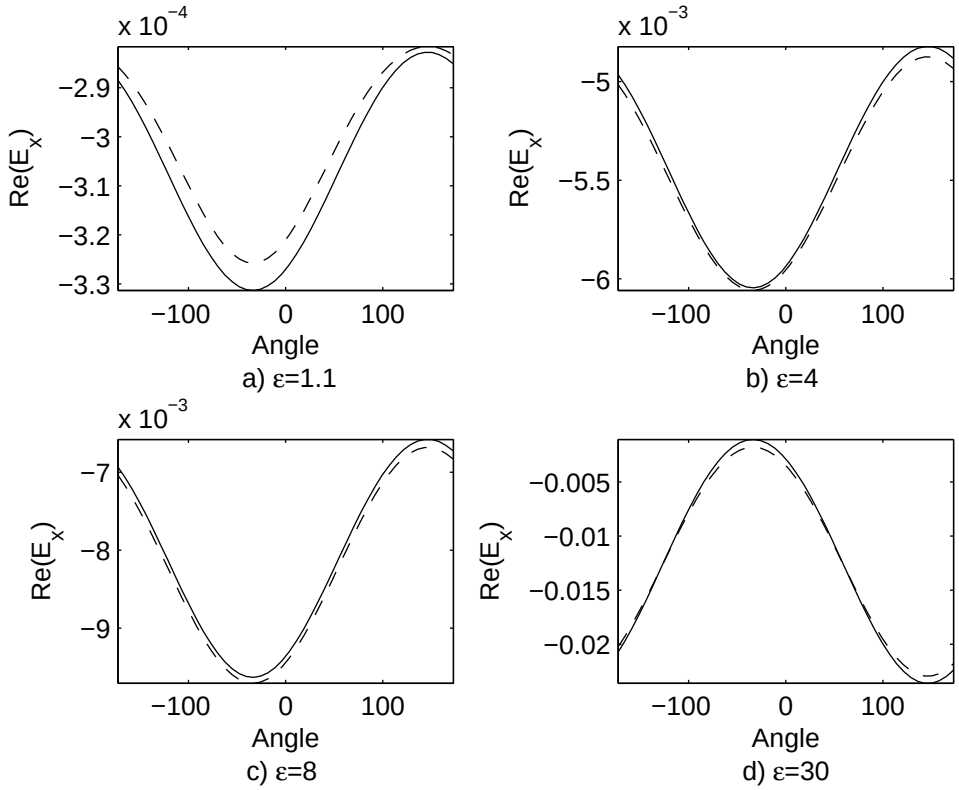

Figure 2.11: The Müller and Mie method comparison for dielectric sphere for different ε. Solid line is the field due to Mie method and dashed is due to Müller method.

Chapter 3

Application on shape optimisation

In this chapter the EFIE formulation for PEC patch is applied to optimise the directivities of wire antennas of different lengths. The optimisation is done with respect to deformation of the antenna by splines. The discussion about whether of not the optimal shape is global is excluded for it is beyond the scope of this thesis. Thus whenever shape is said to be optimal it means that the optimisation algorithms stopping criterion is fulfilled.

Such optimisation process is inspired by Landstorfer's article [19]. Some similar shapes are found in this thesis but for the most part the optimal shapes presented in this paper differ.

The rest of the chapter is organised as follows. In first section the problem is modelled using RWG elements and the optimisation problem is posed. In the second section the optimisation results are presented and in the third and final section the results and methods are compared to those of Landstorfer.

3.1 Problem modelling and posing

Five different antenna lengths are studied: $\frac{1}{2}\lambda$, 1λ, $\frac{3}{2}\lambda$, 2λ and $\frac{5}{2}\lambda$. The geometry of the wire antennas is modelled by a surface patch of width $\frac{\lambda}{50}$ except for the case of $\frac{1}{2}\lambda$ where width $\frac{\lambda}{100}$ is used. The patch lies on xy-plane.

Two different meshes, coarse and fine, are used in order to verify the optimised result. First the shape is sought using coarse mesh and when the optimisation algorithm stops the fine mesh is used. The meshes are depicted in figure 3.1. The coordinate system is also presented in the same figure.

It should be noted that in width direction there are only 2 elements and thus the singular behaviour of the surface current near the edges is not modelled at all. It turns out that current that flows in x direction is negligible compared to that which flows in yz direction and thus the plate model is justified model for a wire antenna. Somewhat better choice element choice might have been rectangular elements since

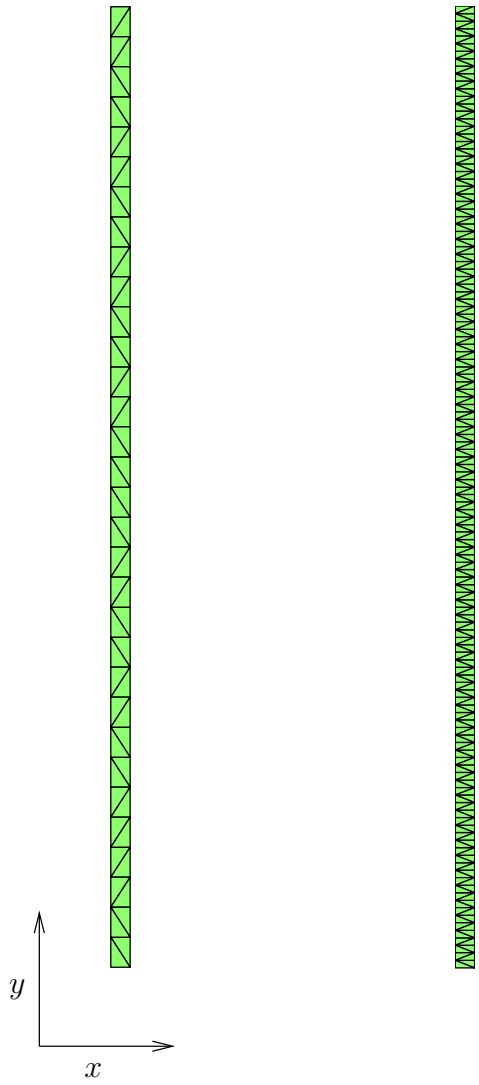

Figure 3.1: Coarse and fine meshes for antenna and the coordinate system.

in that case the current in x direction would have been forced to 0.

The input of the antenna is modelled so that the right hand side's vector's entries corrosponding to the edges that lie in the plane $y = 0$ were set 1 or -1, depending of the edges orientation, and all the other entries were set to 0. This corresponds to a situation where the antenna is fed with $1V$ voltage source at the centre.

The directivity D was measured to the direction of z axis using the formula

$$D = \frac{4\pi \left|\left|\mathbf{E}(\mathbf{r})\right|\right|^2}{\int_S \left|\left|\mathbf{E}(\mathbf{r}')\right|\right|^2 d\mathbf{r}'}, \tag{3.1}$$

where S is a sphere with radius of $10^3\lambda$ and $\mathbf{r} = 10^3\lambda\mathbf{u}_z$. For motivation of such definition of directivity see [20], [21].

Let $X^1 \in \mathbb{R}^{2N+1}$, where $2N+1$ is the dimension of the data that define the deformation and let $X^2_n = n\frac{L}{2N}$, $n = -N, -N+1, \ldots, 0, 1, \ldots, N$, where L is the length of the patch. The array X^1 is called the node data and X^2 the node locations. The deformation is defined as a composition three functions: a not-a-knot spline $\sigma : \mathbf{p}_z = \sigma(\mathbf{p}_y)$, such a scaling in y direction that the arc-length of the patch is preserved and such a translation that $\sum_u \mathbf{p}^i_z = 0$.

Furthermore, to obtain a symmetric antenna one can discard half of the node locations and node data by requiring that $X^1_{N-n} = X^1_{N+n}$. Thus $N+1$ numbers completely define the deformation. These numbers are denoted by vector X.

Let $D : \mathbb{R}^{N+1} \to \mathbb{R}^+$ be the directivity of the antenna that has the deformation defining vector as an argument. Thus the problem can be posed as follows:

Problem 3.1 *Find $X \in \mathbb{R}^{N+1}$ such that*

$$\left| D(X) - \sup_{\tilde{X}} D(\tilde{X}) \right| + ||(\nabla D)(X)|| \tag{3.2}$$

is small.

However, since one does not know the $\sup_{\tilde{X}} D(\tilde{X})$ one can only try to maximise the directivity and stop the maximisation algorithm when $||(\nabla D)(X)||$ is small or the norm of the difference between successive values of X is small.

3.2 Optimisation and results

The optimisation is carried out using slightly modified BFGS (Broyden, Fletcher, Goldfarb and Shanno) method with Armijo backtracking line search. For overview of these methods, see [22]. The modified method is described in Appendix B in greater detail.

The dimension of deformation the defining vector was chosen after some experimenting to be 17. For equidistant node locations this choice puts node on every vertex

Table 3.1: Summary of optimal shapes.

Length / λ	Directivity / dB	Figures	Linear antenna dir. / dB
$\frac{1}{2}$	2.2	3.2, 3.3	2.2
1	4.3	3.4, 3.5	4.0
$1\frac{1}{2}$	7.1	3.6, 3.7	-1.9
2	7.5	3.8, 3.9	-19
$2\frac{1}{2}$	9.2	3.10, 3.11	0.8

on the coarse mesh on the yz-plane. Thus choosing greater dimension would force one to choose also finer mesh as the coarse mesh.

The shape, directivity pattern in the yz-plane, projection of current density in to the yz plane on the antenna and orthographic projection of the current density as colour plot of each of the antennas are visualised in figures 3.2 - 3.11.

The current distributions plots are parametrised by arc-length to be able to compare the current distribution to the sinusoidal current distribution approximation of the thin linear antenna [20], [21]. Although it's quite challenging for most of the part to compare the current distributions to sinusoidal approximations the difference is very clear at antenna lengths $1\frac{1}{2}\lambda$ and up. The difficulty is due to the fact that current density is complex vector field on the surface and the approximations are not presented in modulus-argument $z(t) = |z(t)|e^{i\phi(t)}$ but in the form $z(t) = r(t)e^{i\varphi(t)}$, where $r, \phi, \varphi : \mathbb{R} \to \mathbb{R}$.

For comparison, the current distributions of straight antennas are presented in figures 3.12 (a-e).

The optimal directivities in decibels and references to figures are presented in table 3.2.

It should be noted that for antenna lengths $\frac{1}{2}\lambda$ and 1λ the algorithm couldn't find substantially better antenna shapes. For all the other antenna shapes the difference is dramatical.

3.2.1 Comparison with Landstorfer's antennas

In article [19] there are presented three antennas of lengths $1\frac{1}{2}\lambda$, 2λ and $2\frac{1}{2}\lambda$. A scan from Landstorfer's article presenting his antennas is in figure 3.13.

Landstorfer used the sinusoidal approximation for current distribution which may be questioned by looking the current distribution of antennas found in this thesis. For antenna length $1\frac{1}{2}\lambda$ the antennas are strikingly similar, cf. figure 3.14. However, for other antenna lengths the differences are remarkably visible. The biggest difference is at antenna length $2\frac{1}{2}$, cf. figures 3.10 and 3.13.

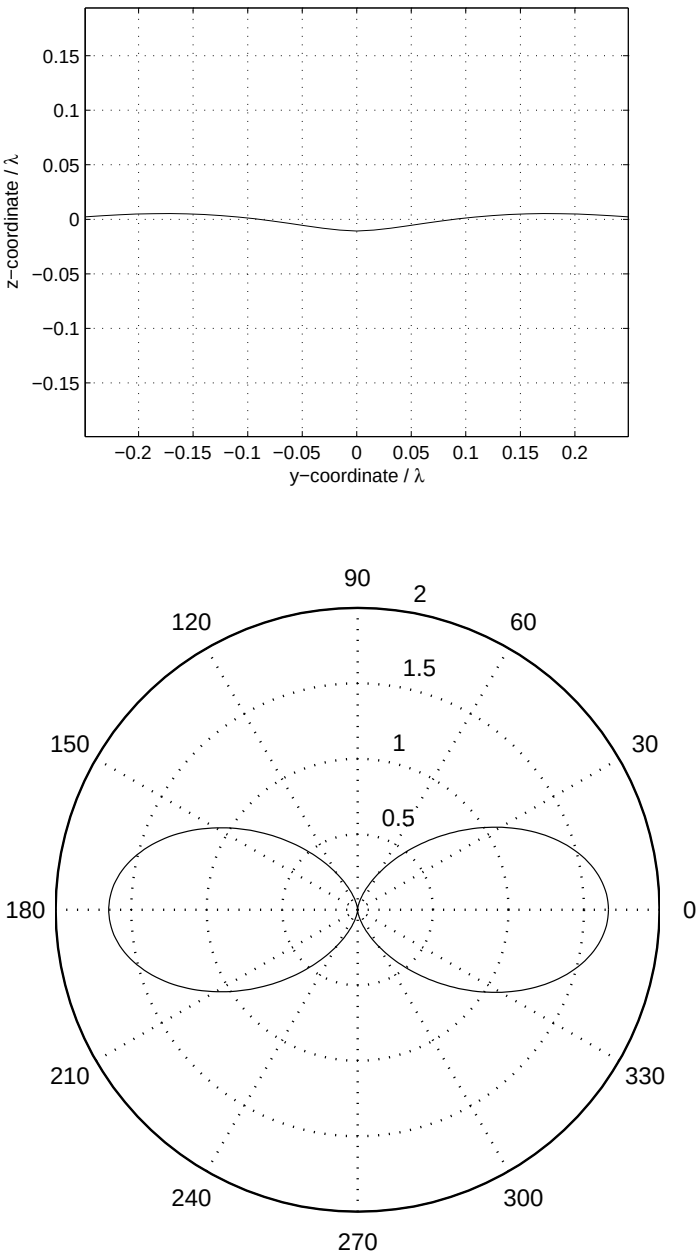

Figure 3.2: Shape and directivity pattern of half wave wire antenna.

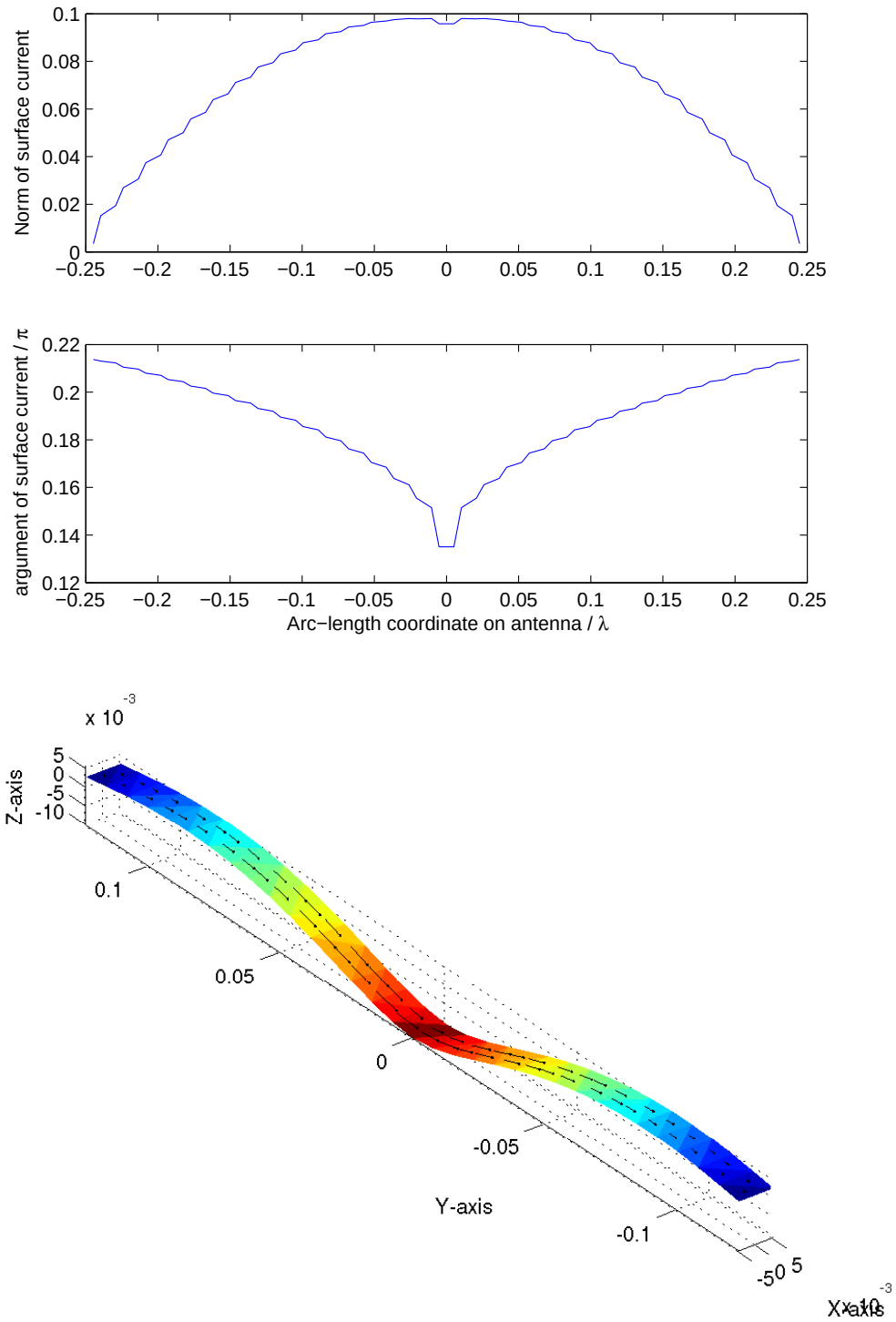

Figure 3.3: Current distribution on half wave antenna along arc length and on 3d visualisation.

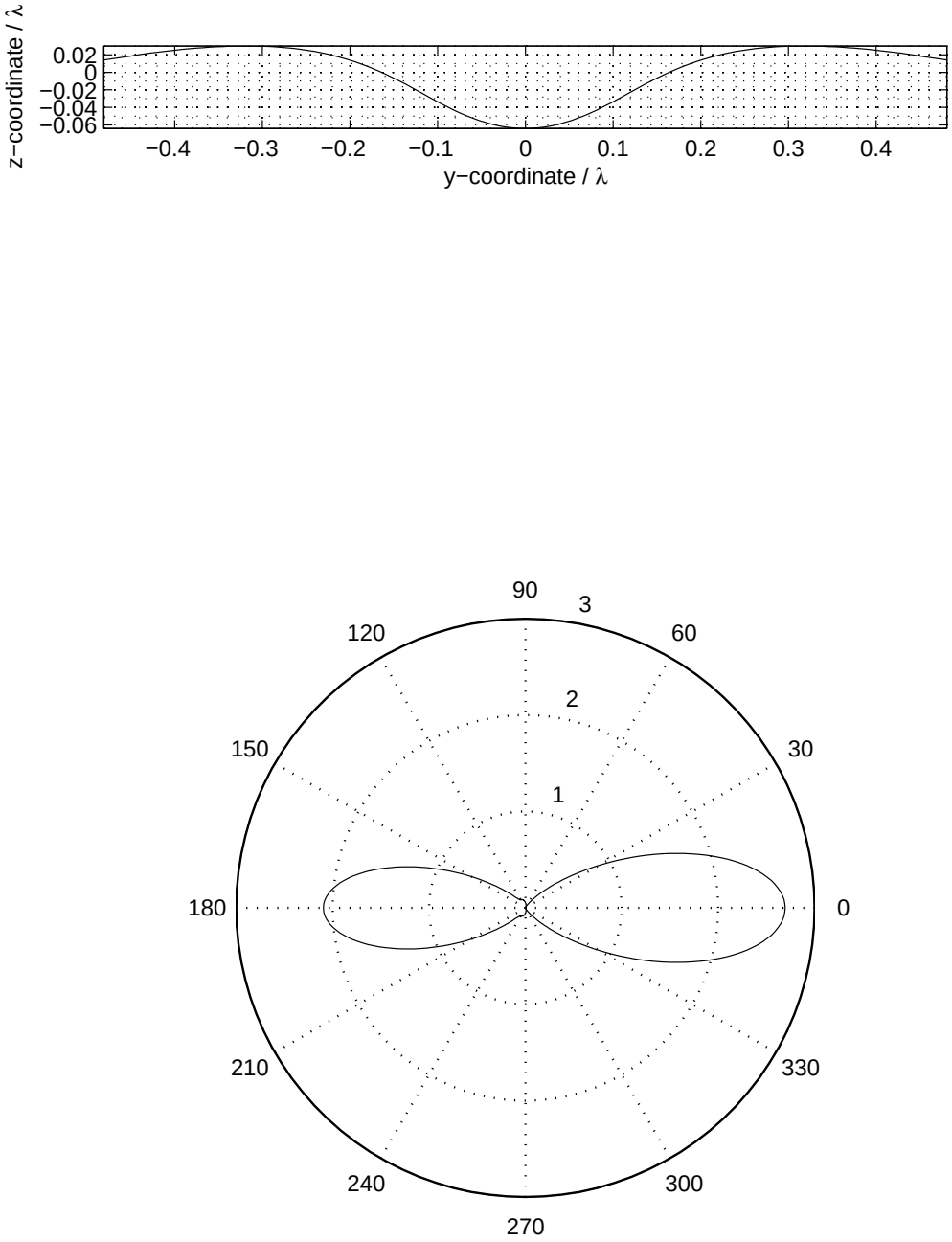

Figure 3.4: Shape and directivity pattern of full wave wire antenna.

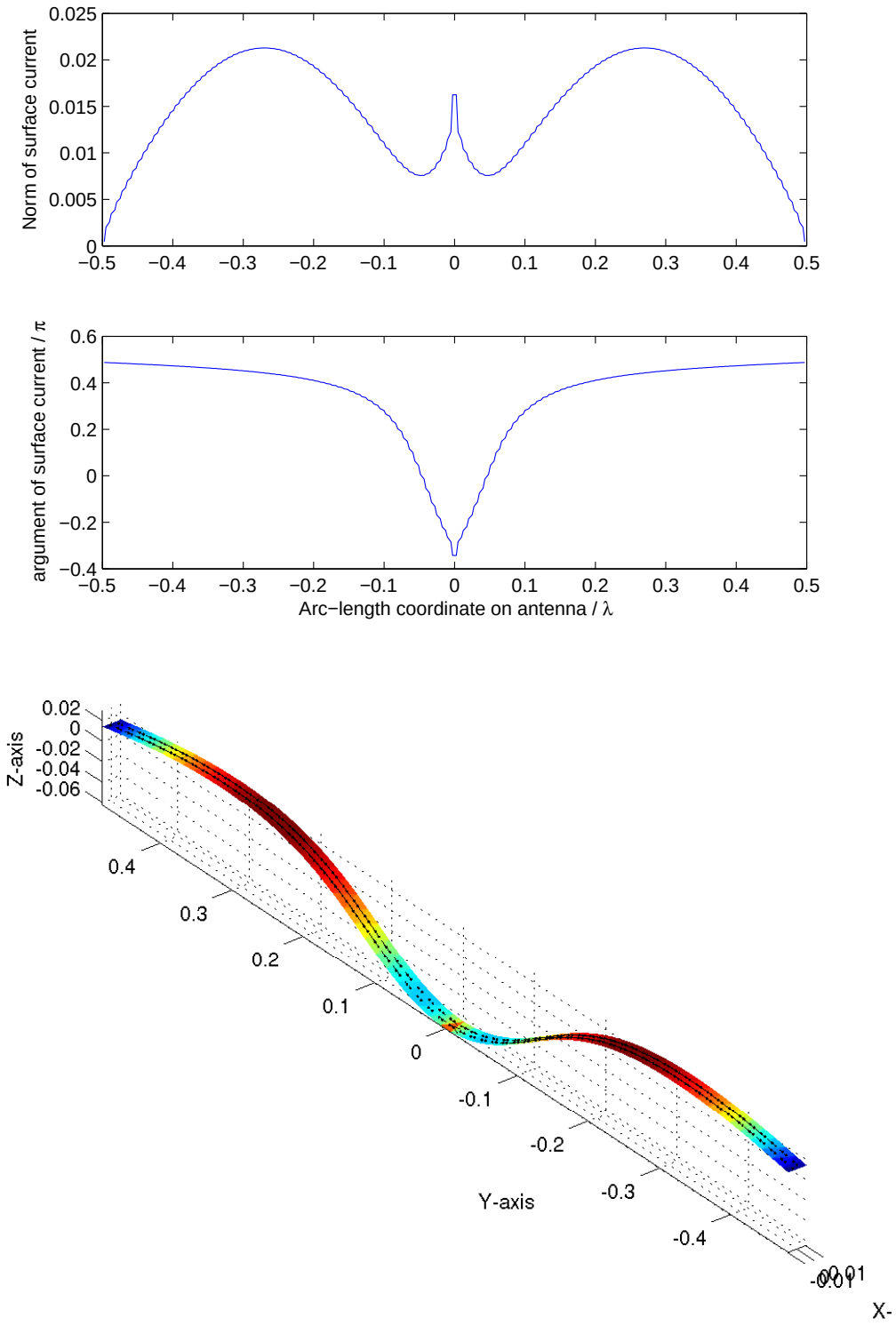

Figure 3.5: Current distribution on full wave antenna along arc length and on 3d visualisation.

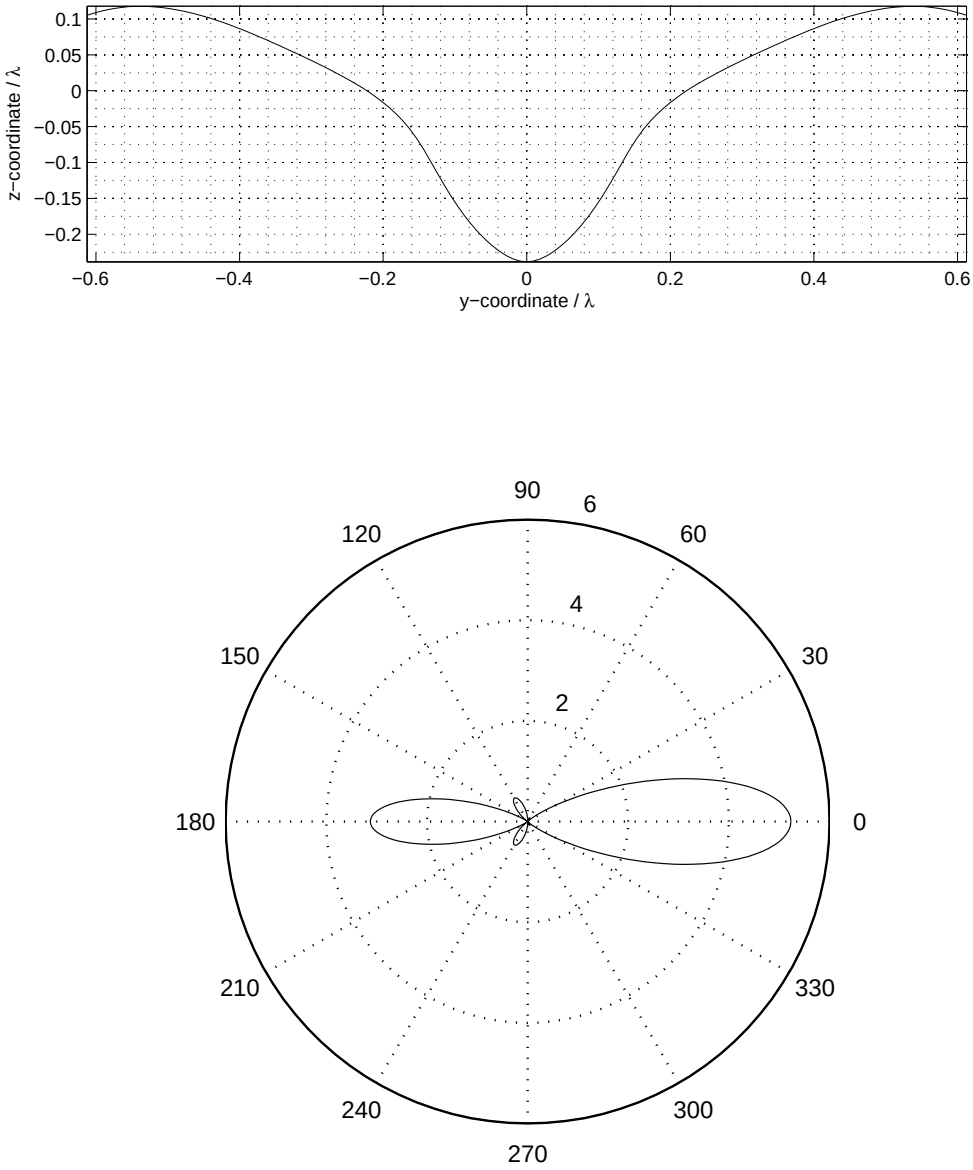

Figure 3.6: Shape and directivity pattern of $1\frac{1}{2}$-wave wire antenna.

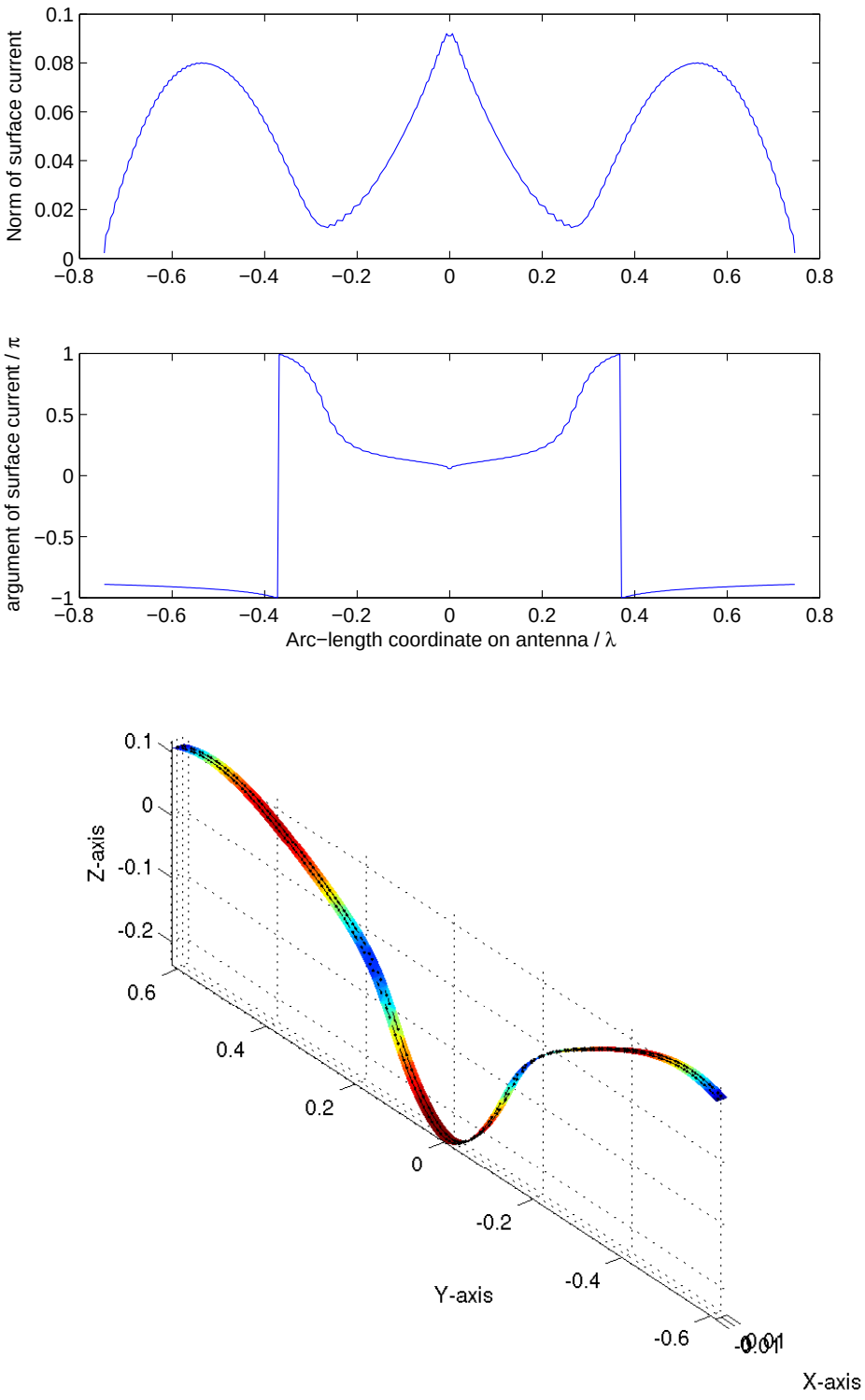

Figure 3.7: Current distribution on $1\frac{1}{2}$-wave antenna along arc length and on 3d visualisation.

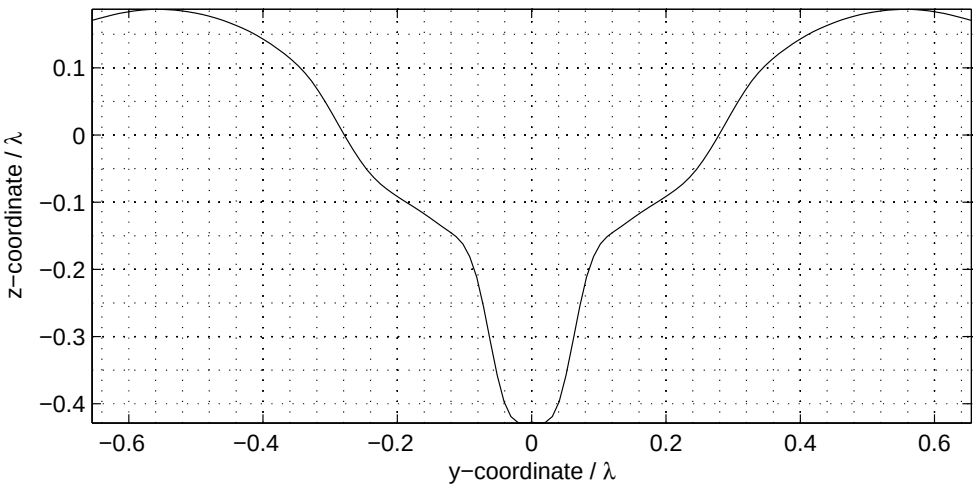

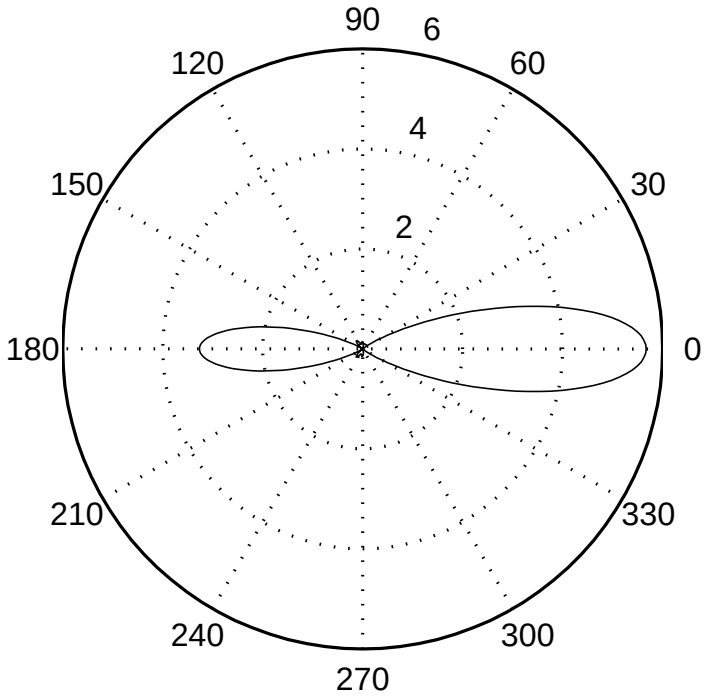

Figure 3.8: Shape and directivity pattern of 2-wave wire antenna.

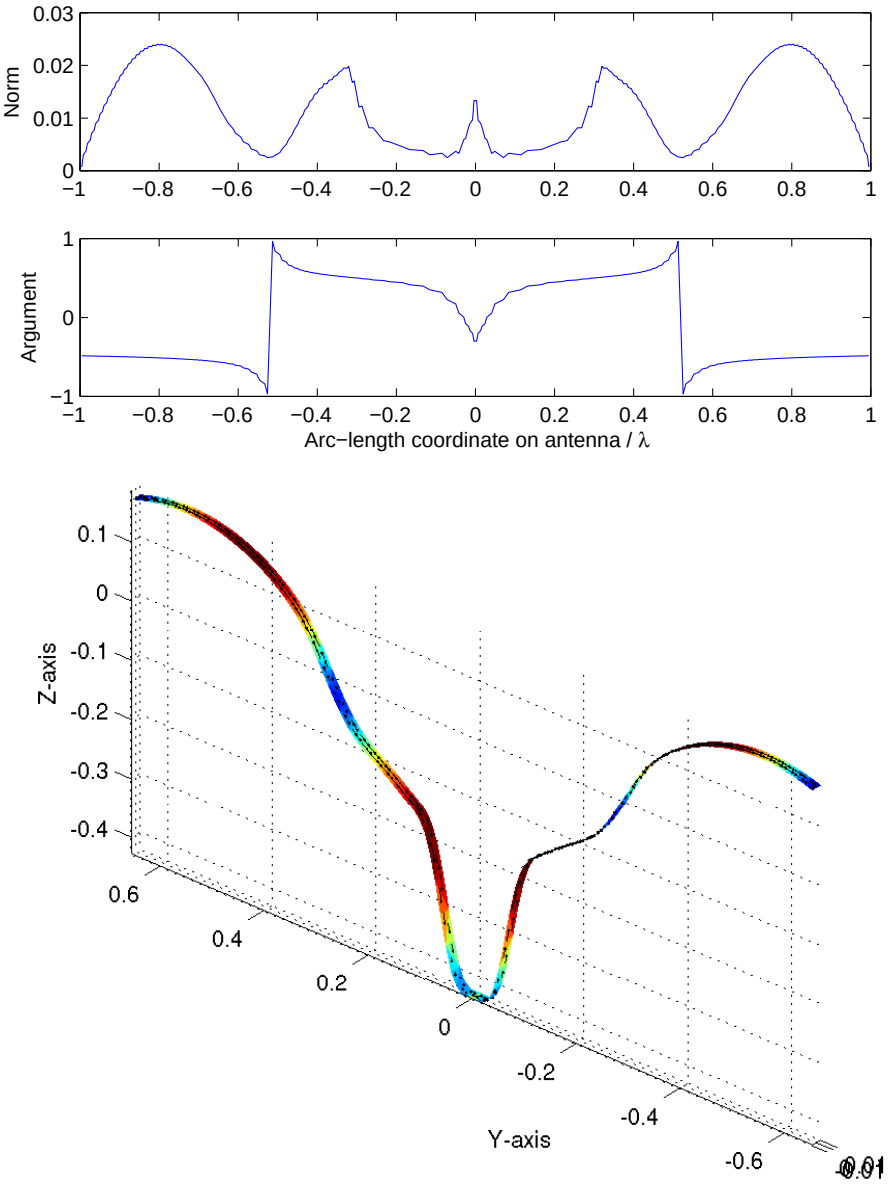

Figure 3.9: Current distribution on 2-wave antenna along arc length and on 3d visualisation.

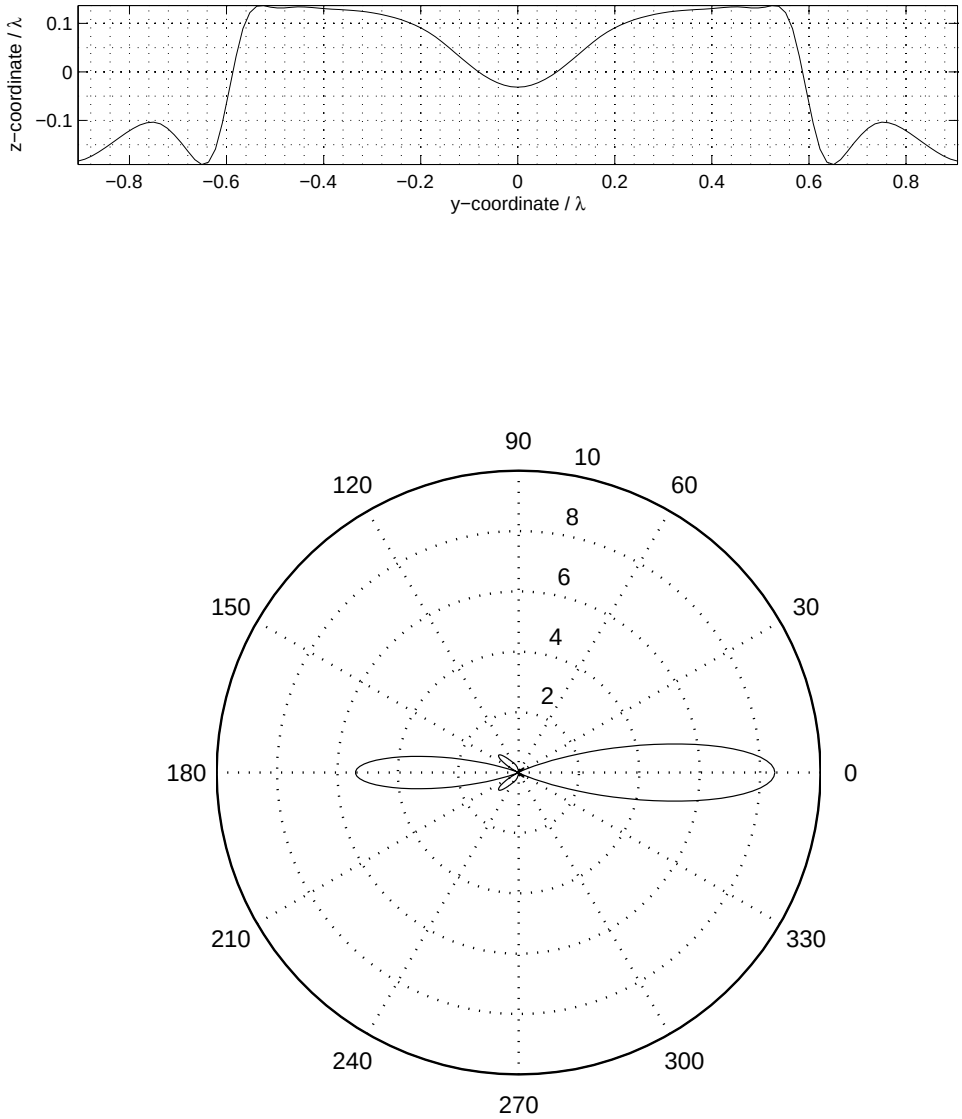

Figure 3.10: Shape and directivity pattern of $2\frac{1}{2}$-wave wire antenna.

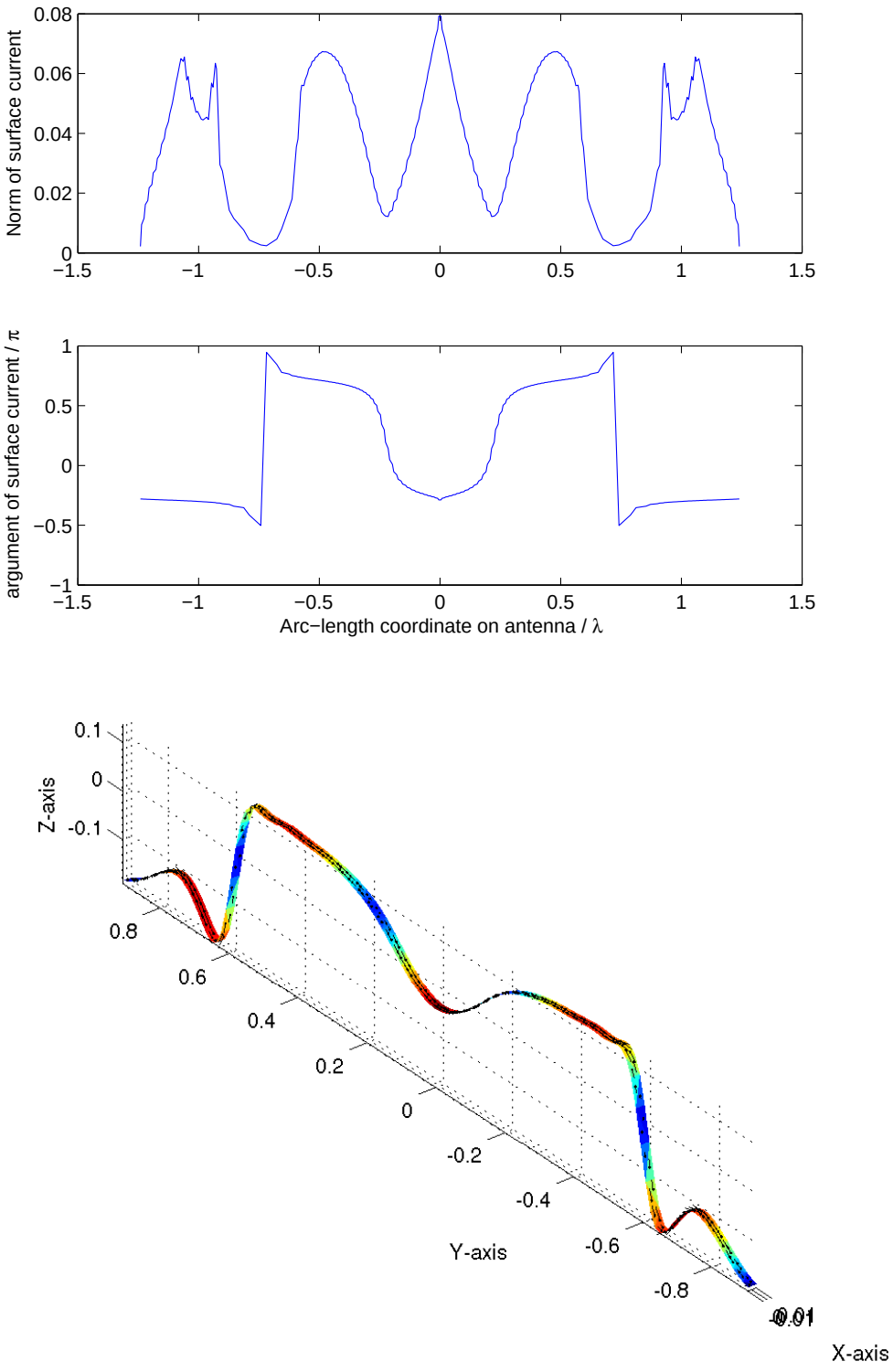

Figure 3.11: Current distribution on $2\frac{1}{2}$-wave antenna along arc length and on 3d visualisation.

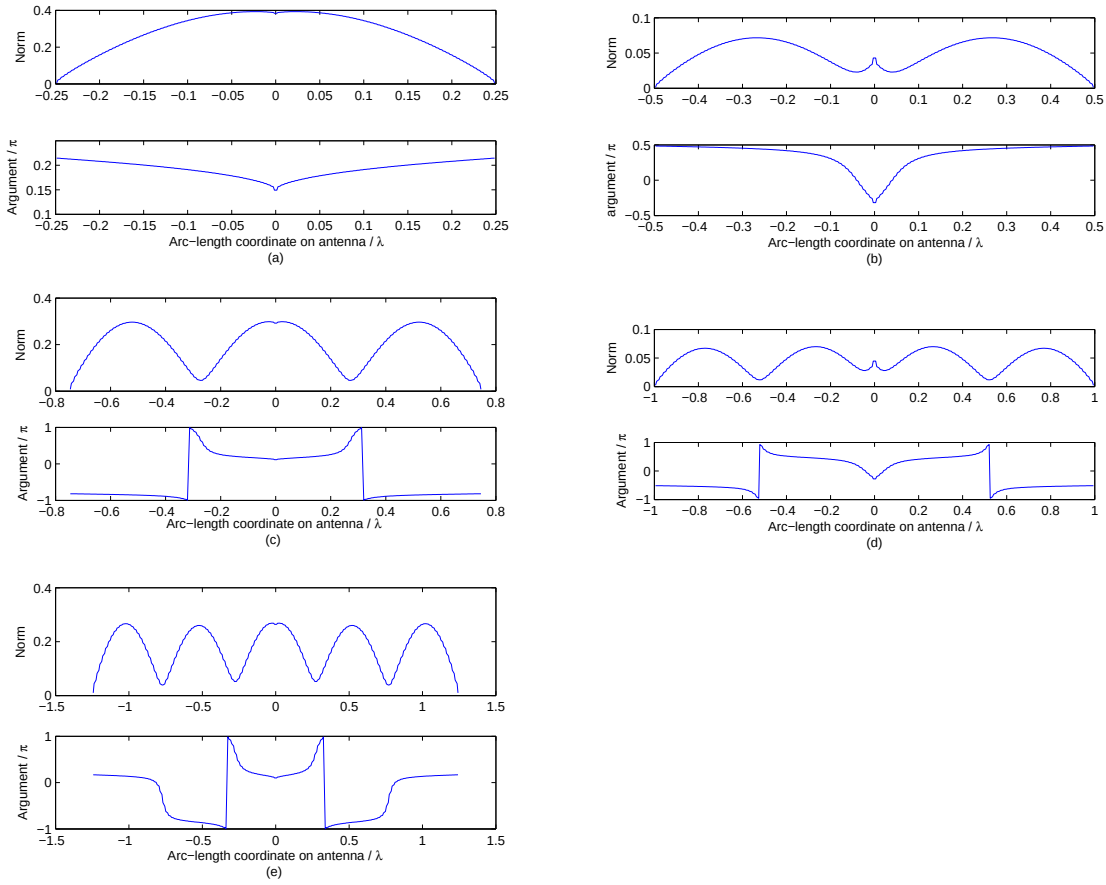

Figure 3.12: Current distributions on straight antennas for antenna lengths $(\frac{1}{2}\lambda, \ldots, 2\frac{1}{2}\lambda)$ in figures (a-e), respectively.

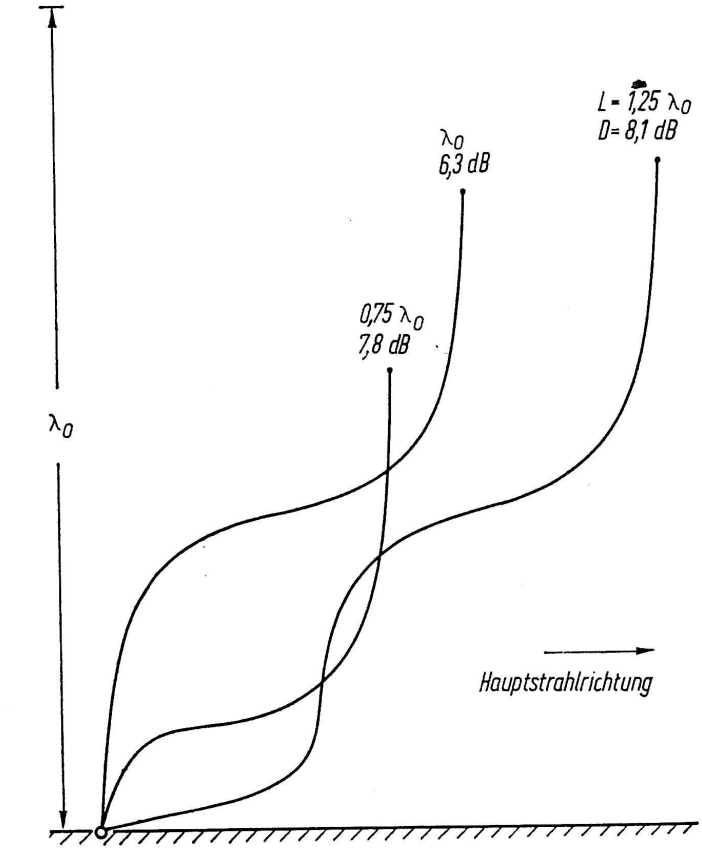

Optimale Gestalt von Linearantennen verschiedener Größe

Figure 3.13: Landstorfer's antennas.

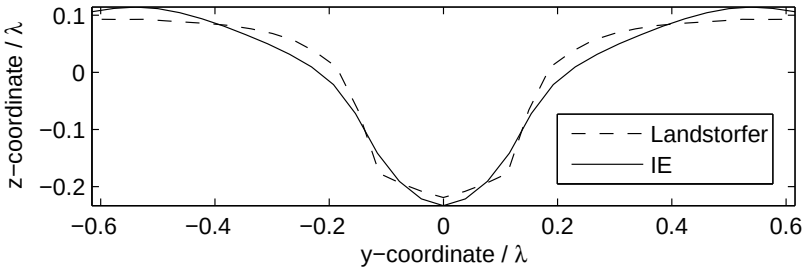

Figure 3.14: Comparison between antenna shapes found in this thesis and by Landstorfer. The antenna length is $1\frac{1}{2}\lambda$.

Chapter 4

Conclusions and future study

It was found that the boundary integral equations are indeed useful tools for analysing electromagnetic scattering from homogeneous objects. The full system matrix does not cause too much problems when the system size is not too large. On modern personal computers the size of the system may be about 5000 DOFs for problems where the system matrix stays constant and about 500 DOFs for variable system matrix problems, such as antenna shape optimisation. With help of fast methods (such as MLFMA) the Müller's formulation is an attractive choice for solving large problems due to it's good iterative properties at a wide frequency range.

By looking at the condition number of the EFIE system matrix it was possible to locate the interior resonance frequencies of such a resonator that has the same boundary as the original scattering object. However, the searching of those frequencies is very slow by calculating the condition number by varying frequencies over some interval. This procedure raises the question if the resonance frequency problem could be treated some way as a very general eigenvalue problem:

Problem 4.1 *Find* $k \in \mathbb{R}^+$ *and* $\mathbf{J}_h \in U_{\mathcal{T}}$ *such that*

$$P\tilde{D}_k(\mathbf{J}_h) = 0,$$

where P *is the projection onto* $V_{\mathcal{T}}$.

A similar question is how stable is the scattered field with respect to small deformations of the scattering mesh and, in the case of curved surfaces, how densely the surface must be triangulated in order to achieve reasonable accuracy. Some hints on the former question was obtained in the process of shape optimisation. There seem to be critical points of the directivity in the deformation parameter space. At the critical points the directivity doesn't change much when the shape of the scatterer is deformed. The latter question was studied by comparing the series solution to solution of the discretized boundary integral equation. But these numerical studies were only a glimpse of the behaviour of the boundary integral equations. No analytical bounds for the error were studied. There is probably something to discover by analysing these questions in a mathematically rigorous fashion.

The EFIE formulation seems to converge quite slowly in the presence of small elements and when using iterative solvers, it seems to be important to be able to precondition the system equation somehow. As the EFIE formulation is a valid method for solving scattering from plates it seems worthwhile to develop preconditioners, which target on the problem of low-frequency breakdown.

Appendix A

Derivation of EFIE$_i$ and MFIE$_i$

Let $\mathbf{E}_s$, $\mathbf{H}_s$ satisfy the exterior Stratton-Chu (Ext-SC) formulas with $k = k_1$ corresponding to $\mathbf{J}_s$ and $\mathbf{M}_s$ and let $\mathbf{E}_p$ and $\mathbf{H}_p$ satisfy the interior Stratton (Int-SC) formulas with $k = k_1$ corresponding to $\mathbf{J}_p$ and $\mathbf{M}_p$. Let $\mathbf{E}_2$, $\mathbf{H}_2$ satisfy the Int-SC with $k = k_2$.

The fields $(\mathbf{E}_s, \mathbf{H}_s)$ and $(\mathbf{E}_p, \mathbf{H}_p)$ are such that their sum satisfies the Maxwell's equations in the presence of the scattering object. The sum is denoted by $(\mathbf{E}_1, \mathbf{H}_1)$.

Thus it holds

$$-\frac{1}{i\omega\varepsilon_1} D_{k_1}(\mathbf{J}_s) - K_{k_1}(\mathbf{M}_s) = \mathbf{E}_s, \quad \text{in } extD \tag{A.1}$$

$$-\frac{1}{i\omega\mu_1} D_{k_1}(\mathbf{M}_s) + K_{k_1}(\mathbf{J}_s) = \mathbf{H}_s, \quad \text{in } extD \tag{A.2}$$

$$-\frac{1}{i\omega\varepsilon_1} D_{k_1}(\mathbf{J}_p) - K_{k_1}(\mathbf{M}_p) = 0, \quad \text{in } extD \tag{A.3}$$

$$-\frac{1}{i\omega\mu_1} D_{k_1}(\mathbf{M}_p) + K_{k_1}(\mathbf{J}_p) = 0, \quad \text{in } extD \tag{A.4}$$

$$-\frac{1}{i\omega\varepsilon_1} D_{k_2}(\mathbf{J}_2) - K_{k_2}(\mathbf{M}_2) = 0, \quad \text{in } extD \tag{A.5}$$

$$-\frac{1}{i\omega\mu_1} D_{k_2}(\mathbf{M}_2) + K_{k_2}(\mathbf{J}_2) = 0, \quad \text{in } extD. \tag{A.6}$$

Summing up (A.1) + (A.3) and (A.2) + (A.4) and using the fact that the tangential components of the fields continuous across the boundary one is left with four

equations

$$-\frac{1}{i\omega\varepsilon_1}D_{k_1}(\mathbf{J}) - K_{k_1}(\mathbf{M}) = \mathbf{E}_s, \quad \text{in } extD \tag{A.7}$$

$$-\frac{1}{i\omega\mu_1}D_{k_1}(\mathbf{M}) + K_{k_1}(\mathbf{J}) = \mathbf{H}_s, \quad \text{in } extD \tag{A.8}$$

$$-\frac{1}{i\omega\varepsilon_1}D_{k_2}(\mathbf{J}) - K_{k_2}(\mathbf{M}) = 0, \quad \text{in } extD \tag{A.9}$$

$$-\frac{1}{i\omega\mu_1}D_{k_2}(\mathbf{M}) + K_{k_2}(\mathbf{J}) = 0, \quad \text{in } extD. \tag{A.10}$$

Then multiplying each of the equations (A.7-A.10) by $\hat{\mathbf{n}}\times$ from left and taking the limit (using limiting theorem 1.3) to the boundary one obtains the following set of equations:

$$-\frac{1}{i\omega\varepsilon_1}\tilde{D}_{k_1}(\mathbf{J}) - \tilde{K}_{k_1}(\mathbf{M}) - \frac{1}{2}\mathbf{M} = \hat{\mathbf{n}}\times\mathbf{E}_s, \tag{A.11}$$

$$-\frac{1}{i\omega\mu_1}\tilde{D}_{k_1}\mathbf{M} + \tilde{K}_{k_1}(\mathbf{J}) + \frac{1}{2}\mathbf{J} = \hat{\mathbf{n}}\times\mathbf{M}_s, \tag{A.12}$$

$$-\frac{1}{i\omega\varepsilon_2}\tilde{D}_{k_2}(\mathbf{J}) - \tilde{K}_{k_2}(\mathbf{M}) - \frac{1}{2}\mathbf{M} = 0, \tag{A.13}$$

$$-\frac{1}{i\omega\mu_2}\tilde{D}_{k_2}\mathbf{M} + \tilde{K}_{k_2}(\mathbf{J}) + \frac{1}{2}\mathbf{J} = 0. \tag{A.14}$$

Finally since $\hat{\mathbf{n}}\times\mathbf{E}_s = \hat{\mathbf{n}}\times\mathbf{E} - \hat{\mathbf{n}}\times\mathbf{E}_p$ and $\hat{\mathbf{n}}\times\mathbf{H}_s = \hat{\mathbf{n}}\times\mathbf{H} - \hat{\mathbf{n}}\times\mathbf{H}_p$ and using the definition (1.14) of $\mathbf{M}$ and $\mathbf{J}$ the final four equations are obtained.

Appendix B

The BFGS-algorithm

Let $f : \mathbb{R}^n \to \mathbb{R}$ be differentiable. Denote $\nabla_h f(x) := \sum_i (f(x + he_i) - f(x))/h$ the numerical (forward) derivative of f in point x. Let H_0 be an initial guess for the inverse Hessian matrix of f and x_0 be the initial guess of the minimising vector. These can be chosen as $H_0 = I$ and $x_0 = 0$. Denote $f_k = f(x_k)$.

The BFGS-algorithm is now as follows [22]:

$k \leftarrow 0$;
while $||\nabla_h f_k|| > \epsilon$ **do**
  $p_k \leftarrow -H_k \nabla_h f_k$;
  $x_{k+1} \leftarrow x_k + \alpha_k p_k$, where the α_k is the line search parameter so that new guess satisfies the Wolfe conditions;
  $s \leftarrow x_{k+1} - x_k$;
  $y \leftarrow \nabla_h f_{k+1} - \nabla_h f_k$;
  $\rho \leftarrow 1/(y^{\mathrm{T}} s)$;
  $H_{k+1} \leftarrow (I - \rho s y^{\mathrm{T}}) H_k (I - \rho y s^{\mathrm{T}}) + \rho s s^{\mathrm{T}}$;
  $k \leftarrow k + 1$;
end

The modificated BFGS-algorithm used in this thesis is such that line search is required only to satisfy the Armijo condition [22], the difference between smallest and largest element of x is not too big and that any decrease of f is achieved. Additionally, the algorithm is essentially restarted by setting $H_{k+1} = I$ every time $1/\rho$ is smaller than 10^{-9}

Bibliography

[1] D. R. Wilton, S. M. Rao, A. W. Glisson, D. H. Schaubert, O. M. Al-Bundak, and C. M. Butler, "Potential integrals for uniform and and linear source distributions on polygonal and polyhedral domains," *IEEE Transactions on Antennas and Propagation*, vol. AP-32, no. 3, pp. 276–281, 1984.

[2] R. Graglia, "On the numerical integration of the linear shape functions times the 3-d green's function or its gradient on a plane triangle," *Antennas and Propagation, IEEE Transactions on*, vol. 41, no. 10, pp. 1448–1455, Oct 1993.

[3] I. Hänninen, M. Taskinen, and J. Sarvas, "Singularity subtraction integral formulae for surface integral equations with rwg, rooftop and hybrid basis functions," *IEEE Transactions on Antennas and Propagation*, vol. 53, October 2005.

[4] S. Järvenpää, M. Taskinen, and P. Ylä-Oijala, "Singularity subtraction technique for high-order polynomial vector basis functions on planar triangles," *IEEE Transactions on Antennas and Propagation*, vol. 54, pp. 42–49, January 2006.

[5] Y. Saad and M. H. Schultz, "GMRES: A generalized minimal residual algorithm for solving nonsymmetric linear systems," *SIAM Journal on Scientific and Statistical Computing*, vol. 7, no. 3, pp. 856–869, 1986.

[6] L. N. Trefethen and D. Bau, *Numerical Linear Algebra.* SIAM: Society for Industrial and Applied Mathematics, June 1997.

[7] D. Colton and R. Kress, *Integral Equation Methods in Scattering Theory.* John Wiley & Sons, 1983.

[8] J. Sarvas, S. Järvenpää, and P. Ylä-Oijala, "Finite element and integral equation methods in electromagnetic field computing." Lecture notes for the course held by Helsinki Univ. Tech. Electromagnetics laboratory, 2005.

[9] W. C. Chew, *Waves and Fields in Inhomogeneous Media.* IEEE Press, 1995.

[10] J. A. Stratton and L. J. Chu, "Diffraction theory of electromagnetic waves," *Physical Review*, vol. 56, pp. 99–107, July 1939.

[11] P. G. Ciarlet, *The Finite Element Method for Elliptic Problems.* Amsterdam, The Netherlands: North-Holland, 1978.

[12] D. Braess, *Finite elements, Theory, fast solvers, and applications in solid mechanics, Second Edition.* Cambridge University Press, 2001.

[13] S. M. Rao, D. R. Wilton, and A. W. Glisson, "Electromagnetic scattering by surfaces of arbitrary shape," *IEEE Transactions on Antennas and Propagation*, vol. 30, pp. 409–418, May 1982.

[14] P.-A. Raviart and J. M. Thomas, "A mixed finite element method for 2nd order elliptic problems," in *Mathematical aspects of finite element methods (Proc. Conf., Consiglio Naz. delle Ricerche (C.N.R.), Rome, 1975)*, pp. 292–315. Lecture Notes in Math., Vol. 606, Berlin: Springer, 1977.

[15] H. Wallen, S. Järvenpää, P. Ylä-Oijala, and J. Sarvas, "Broadband müller-mlfma for electromagnetic scattering by dielectric objects," *IEEE Transactions on Antennas and Propagation*, vol. 55, no. 5, 2007.

[16] P. Ylä-Oijala and M. Taskinen, "Well-conditioned müller formulation for electromagnetic scattering by dielectric objects," *IEEE Transactions on Antennas and Propagation*, vol. 53, no. 10, 2005.

[17] P. Monk, *Finite Element Methods for Maxwell's Equations.* Clarendon Press, Oxford, UK, 2003.

[18] I. Lindell, *Aaltojohtoteoria.* Otatieto, 1997.

[19] F. Landstorfer, "Zur optimalen form von linearantennen," *Frequenz*, vol. 30, no. 12, pp. 344–349, 1976.

[20] J. D. Kraus and R. J. Marhefka, *Antennas For All Applications.* McGraw-Hill, 3. ed., 2002.

[21] I. Lindell and K. Nikoskinen, *Antenniteoria.* Otatieto, 4. ed., 1995.

[22] J. Nocedal and S. J. Wright, *Numerical Optimization.* Springer, 1999.